

ON THE DECAY OF Br 82

ON THE DECAY OF  $\text{Br}^{82}$

by

IAN BRUCE WEBSTER, B. ENG.

A Thesis

Submitted to the Faculty of Graduate Studies

in Partial Fulfilment of the Requirements

for the Degree

Master of Science

McMaster University

April, 1964

MILLS MEMORIAL  
LIBRARY  
McMASTER UNIVERSITY

MASTER OF SCIENCE (1964)  
(Physics)

McMASTER UNIVERSITY  
Hamilton, Ontario

TITLE:           On the Decay of Br<sup>82</sup>

AUTHOR:           Ian Bruce Webster, B. Eng. (McMaster University)

SUPERVISOR:       Dr. T. J. Kennett

NUMBER OF PAGES:   vii, 57

SCOPE AND CONTENTS:

Single-crystal, pair, and two-dimensional spectro-metry methods have been applied to a study of the decay radiations from 36-hour Br<sup>82</sup>. Two new gamma rays have been discovered and a new energy level in Kr<sup>82</sup> has been established. Double and triple gamma summing is discussed. Also regression analysis techniques for coincidence data analysis have been studied. This has been applied to the case of Br<sup>82</sup> to derive gamma ray intensities.

#### ACKNOWLEDGEMENTS

I wish to express appreciation to my Research Director, Dr. T. J. Kennett, for his guidance and assistance throughout this work. I would also like to thank Dr. W. V. Prestwich for his part in the experimentation and in the development of the theory for the Regression Analysis and Dr. G. L. Keech for helping in the preparation of the computer program.

## TABLE OF CONTENTS

	Page
CHAPTER I      INTRODUCTION	1
1.1    Purpose and Background	1
1.2    Sample Preparation	3
CHAPTER II      EXPERIMENTAL TECHNIQUES	4
2.1    Single-Crystal Spectrometry	4
2.2    Summing Effects	7
(a) Coincidence and Random Summing	7
(b) Bremsstrahlung	13
2.3    Pair Spectrometry	13
(a) The Spectrometer	13
(b) Efficiency and Resolution	16
2.4    Two-Dimensional Coincidence Spectrometry	20
CHAPTER III    Br <sup>82</sup> DECAY SCHEME	26
3.1    Single Spectrum	26
3.2    Pair Spectrum	28
3.3    Coincidence Spectrum	28
3.4    Revised Decay Scheme	33
(a) Energies	33
(b) Intensities	36
CHAPTER IV      REGRESSION ANALYSIS	39
4.1    Reduction of Coincidence Surface	39
(a) Outline	39
(b) Analysis of Coupled Equations	40
(c) Analysis of Original Model Equation	41
(d) Error Estimate	42
(e) Physical Significance of the Variance	44
4.2    Intensities from Intensity Correlation Matrix	44
4.3    Br <sup>82</sup> Gamma-Ray Intensities	47
(a) Data Collection	47
(b) Preparation of Line Shapes and Surface Reduction	49
(c) Results	53
4.4    Conclusions	55
REFERENCES	57

## LIST OF TABLES

Number	Title	Page
I	New Gamma-Ray Energies for Br <sup>82</sup>	33
II	Some Gamma-Ray Intensities for Br <sup>82</sup>	38
III	Theoretical Intensity Correlation Matrix	48
IV	Matrix Elements Values	54
V	Br <sup>82</sup> Intensities from Regression Analysis	55

## LIST OF ILLUSTRATIONS

Figure Number	Title	Page
1.	Previous Decay Scheme for Br <sup>82</sup>	2
2.	Single-Crystal Gamma Ray Response	8
3.	Sum-Coincidence System	11
4.	Double and Triple Cascades	10
5.	Three-Crystal Pair Spectrometer System	14
6.	Pair Spectrum of Na <sup>24</sup> 2.76 MeV $\gamma$ -Ray	17
7.	Pair Cross Section Curve	19
8.	One-Dimensional Coincidence System	21
9.	Sc <sup>46</sup> Decay Scheme	23
10.	Ideal Two-Dimensional Coincidence Array for Sc <sup>46</sup>	23
11.	Two-Dimensional Coincidence Spectrum for Sc <sup>46</sup>	25
12.	Single, Sum, and Difference Spectrum for Br <sup>82</sup>	27
13.	Pair Spectrum for Br <sup>82</sup>	29
14.	Coincidence Spectrum with 1648 keV $\gamma$ -Ray	31
15.	Reduction of 1648 keV Coincidence Array	32
16.	Quadrupole Vibrational Spectrum for Even-Even Nuclei with Spherical Equilibrium Shape	34
17.	Revised Decay Scheme for Br <sup>82</sup>	37

Figure Number	Title	Page
18.	Reduction of Coincidence Surface by Regression Analysis	41
19.	Error Curve	45
20.	Br <sup>82</sup> S(x,l)	50
21.	Gaussian Peak Location	51

## CHAPTER I

### INTRODUCTION

#### 1.1 Purpose and Background

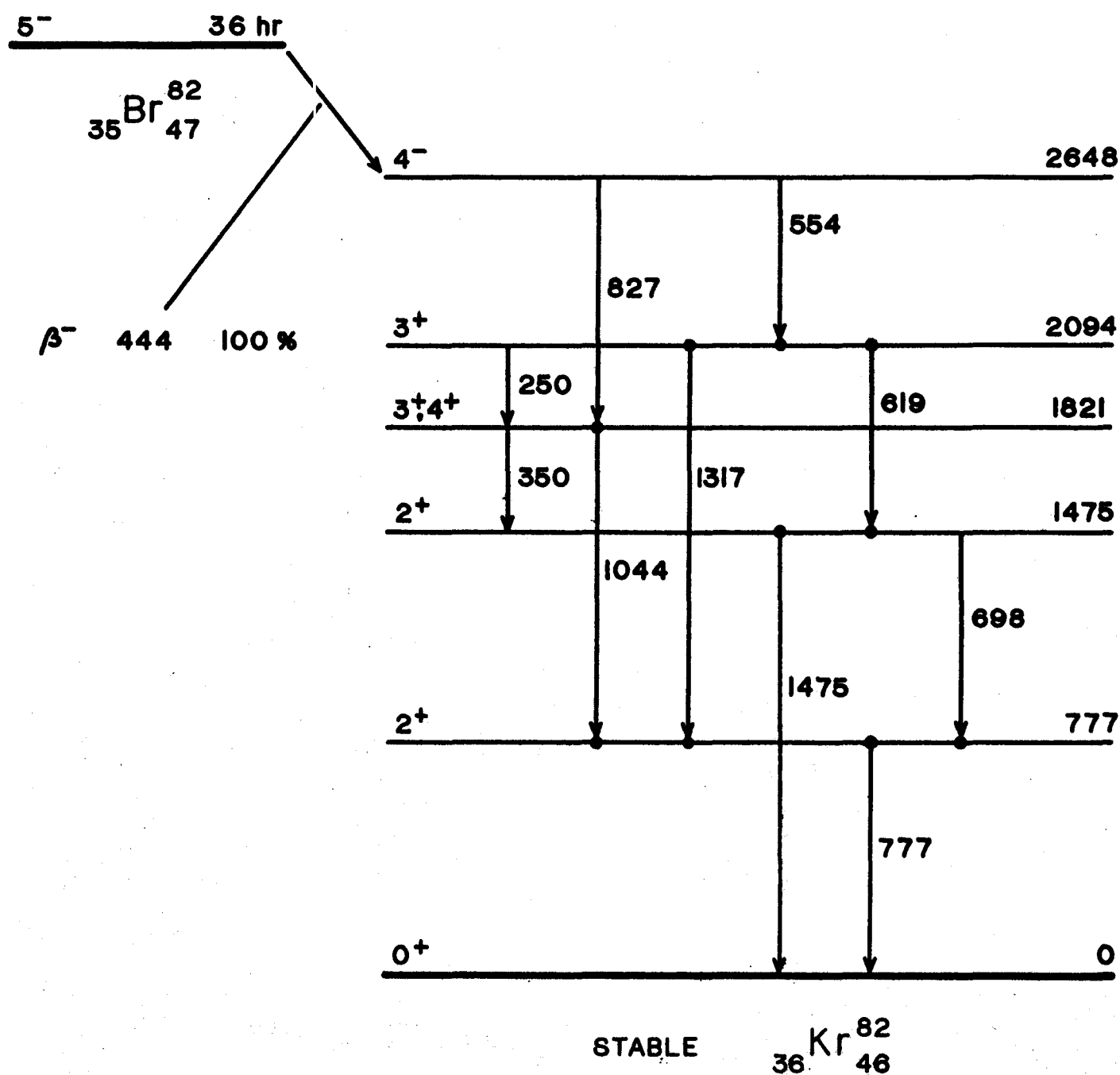
The original purpose of this study was to investigate the application of Regression Analysis to coincidence surfaces in order to obtain gamma-ray intensities.  $\text{Br}^{82}$  was chosen as a test case because, first of all, it was easily obtained without the use of various complicated chemical procedures; secondly, because it had a long half life which avoided the necessity to work quickly and thereby making it possible to ignore lifetime corrections in the data; and thirdly, because the decay scheme had apparently been well investigated.

Gamma-ray energies and level-energy values for  $\text{Br}^{82}$  as summarized by the Nuclear Data Group (1) are shown in Figure 1. A preliminary check on the decay scheme showed what would appear to be an unreported gamma ray at about 1650 keV. It was decided to undertake a more thorough investigation regarding this and the study resulted in a revised decay scheme for  $\text{Br}^{82}$ . It was felt that the methods used and the results obtained in this investigation were of sufficient importance to warrant inclusion in the present work.

FIGURE 1

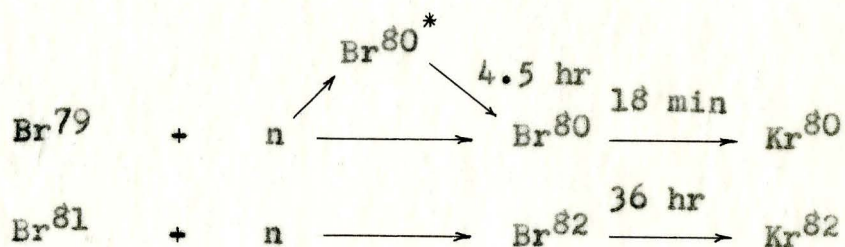
PREVIOUS  $\text{Br}^{82}$  DECAY SCHEME

(ALL ENERGIES IN keV)



## 1.2 Sample Preparation

The  $\text{Br}^{82}$  was produced by neutron irradiation of natural bromine (49%  $\text{Br}^{79}$  and 51%  $\text{Br}^{81}$ ) in the form of  $\text{NH}_4\text{Br}$  in the McMaster Nuclear Reactor. Samples weighing about 75 milligrams were placed in small poly-bags (1/4 inch square) and were irradiated for times of the order of 30 minutes. These were then allowed to decay for three days to ensure the complete decay of the 4.5-hour isomer in  $\text{Br}^{80}$  before any observations were made.



## CHAPTER 11

### EXPERIMENTAL TECHNIQUES

#### 2.1 Single-Crystal Spectrometry

Sodium iodide, activated with thallium, is in general, the most useful inorganic scintillator because of its high fluorescent efficiency, transparency to its own radiation, reasonably short luminescent decay time (0.25  $\mu$ sec) and high sensitivity to gamma rays. (High  $Z=53$  for I increases probability of photoelectric process with respect to Compton scattering.) Such a crystal, optically coupled to a photomultiplier tube (multiplication value about  $10^6$ ) provides an electron current whose total charge is proportional to the initial light intensity. The current pulses give rise to voltage pulses across the anode load. These pass through a linear amplifier and the amplified pulses are then fed to a multi-channel analyzer to complete the system.

When the scintillation spectrometer is used to detect gamma rays, the energy of the gamma radiation is transferred to the electrons in the crystal by a combination of photoelectric, Compton scattering, and pair-producing events, the probabilities of each being energy dependent.

Photoelectric conversion occurs when a gamma ray transfers all its energy to a bound electron. The kinetic energy of the electron is then the energy of the gamma ray less the binding energy of the electron. Immediately an x-ray is produced as a less tightly bound electron drops into the vacancy. The x-ray then interacts with another bound electron, ejecting it, permitting another, lower energy x-ray to be produced and so on, the result being the production of a series of free electrons of decreasing energy whose energies sum to the incident energy.

In Compton scattering, the gamma ray is deflected by a free electron and the energy lost is transferred to the electron, the amount depending on the angle of scattering and being equal to

$$E_e = E_\gamma \left[ 1 - \frac{1}{1 + \alpha(1 - \cos\theta)} \right] \quad \dots (2.1)$$

where  $\alpha = E_\gamma / m_0 c^2$  and  $\theta$  = angle of scattering. If the deflected gamma ray undergoes secondary interactions within the crystal, then the crystal electron energies can total  $E_\gamma$ . But if the gamma ray escapes without further interaction, then the energy deposited to the free electrons in the crystal will lie within the range 0 for  $\theta = 0^\circ$  to a maximum of  $2\alpha E_\gamma / (1 + 2\alpha)$  for  $\theta = 180^\circ$  where the maximum energy is usually the most probable case. Any scattered gamma rays that enter the counter after reflection from surrounding surfaces will, for the most part, have been deflected through an angle greater than  $90^\circ$  hence the

scattered gamma rays will have energies all clustered about 0.2 - 0.5 keV for gamma rays of the order of 1 - 2 MeV. If these scattered gamma rays are then completely detected, they will produce electrons in this energy range.

When the gamma-ray energy exceeds  $2m_0c^2$ , the gamma ray can, in the field of a nucleus, spontaneously convert to an electron-positron pair with total kinetic energy equal to the excess of gamma energy over  $2m_0c^2$ . The positron is slowed down by inelastic collisions with electrons and comes to rest where it combines with an electron, giving rise to two 511-keV annihilation gamma rays travelling in opposite directions. These in turn may or may not interact within the crystal. Free electron energies possible within the NaI crystal as a result can be  $E_\gamma$  for total interaction,  $E_\gamma - m_0c^2$  or  $E_\gamma - 2m_0c^2$  for interaction with one or neither of the annihilation gamma rays, or with much smaller probability, any intermediate value.

As a result of these three types of reactions, for each gamma ray entering the NaI crystal, there are a large number of energized free electrons produced. The total energy of these will lie within the total energy range 0 to  $E_\gamma$  but with the energies mentioned above being more probable. The kinetic energy of these charged particles elevates loosely bound valence electrons to the conduction band. Some of these return to the ground state immediately by visible photon emission and others de-excite by radiationless transitions or conversion to heat.

About 10% of the light produced for each gamma ray

effectively produces photoelectrons at the photocathode of the photomultiplier tube. The number of photoelectrons forms a Poisson distribution whose mean value is proportional to the energy of the incident gamma ray deposited within the crystal. Thus the pulse heights recorded by the multi-channel analyzer for the favoured energies will not be unique but will exhibit a spread or distribution. For example, the photopeak response of the crystal to a monoenergetic gamma ray will be blurred out into a Gaussian shape rather than a delta function. Figure 2 shows the spectrometer response to several monoenergetic gamma rays for a 3x3-inch NaI(Tl) crystal. The appropriate spectra show clearly the photopeak at  $E_\gamma$ , pair-spectrum peaks at  $E_\gamma - m_0c^2$  and  $E_\gamma - 2m_0c^2$ , the Compton edge and continuum as well as the backscatter peak.

## 2.2 Summing Effects

### (a) Coincidence and Random Summing

Another contribution to the scintillator response is coincidence and random summing. When the time interval between two or more gamma rays entering the scintillation crystal is less than the effective resolving time of the system, the unresolved events appear as a single event. The pulse height associated with this sum event is a function of the pulse heights associated with each member of the sum and the time interval between them (2).

It is convenient to distinguish between coincidence and random summing which occurs for correlated and uncorrelated events respectively. In coincidence summing, the average

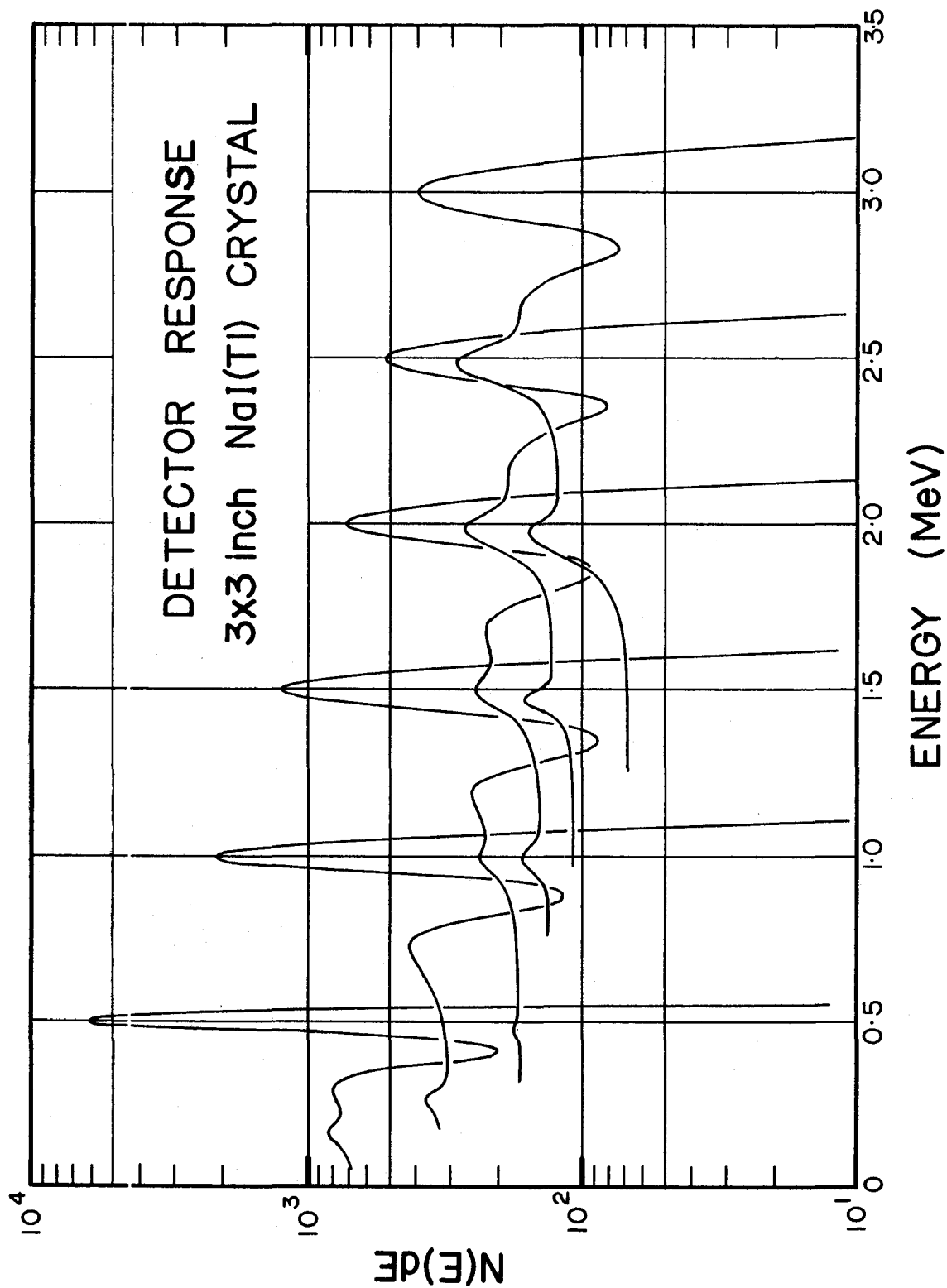


FIGURE 2

time interval between the correlated gamma rays is usually much less than the resolving time of the system. In this case the pulse height of a coincidence sum event is always simply the sum of the pulse heights associated with the members of the correlated event. In random summing the pulse height of the sum event depends on the time interval between the gamma rays and can take on all values between the pulse height for the first gamma event right up to the sum of all pulse heights for all the events involved.

If the single spectrum consists of the set of gamma rays ( $\gamma_i$ ), and if we let  $N_0$  = source strength  
 $e$  = detection efficiency  
 $\Omega$  = subtended solid angle  
 $f$  = fraction of decays  
 $W$  = angular correlation function,  
 $\tau$  = electronic resolving time

then the single crystal counting rate is given by

$$N_s = N_0 \sum_i e_i \Omega_i f_i, \quad \dots (2.2)$$

the coincidence-summing rate is given by

$$N_{cs} = N_0 \sum_{ij} e_i \Omega_i f_i e_j \Omega_j f_j W_{ij}, \quad \dots (2.3)$$

and the random-summing rate is given by

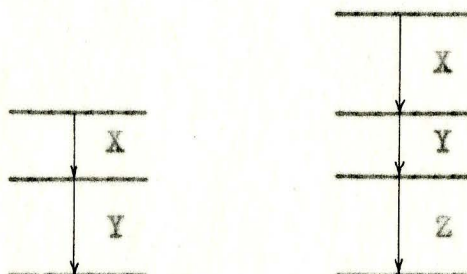
$$\begin{aligned} N_{rs} &= 2\tau N_0^2 \sum_{ij} e_i \Omega_i f_i e_j \Omega_j f_j \quad \dots (2.4) \\ &= 2\tau N_s^2. \end{aligned}$$

Thus since  $\Omega_i = \Omega_j$  when the two crystals have the same geometry, the contribution from coincidence and random summing may be reduced relative to the single-crystal rate by reducing the solid angle and source strength respectively. However, this is not always practical if statistically significant results

are desired.

Instead, an experimental measurement of the sum contribution is readily obtainable. The system employed in this work is shown in Figure 3. (DD2 is a double delay line linear amplifier; S. C. is a slow coincidence circuit; and MCA is an multichannel pulse-height analyzer.) If the resolving time of the slow coincidence circuit is made equal to or greater than the clipping time<sup>\*</sup> of the amplifier, then the routed spectrum consists of both the coincidence-sum and random-sum contributions.

Consider the gamma rays X, Y, and Z. If they are correlated as in Figure 4, then coincidence summing is possible for each decaying nucleus and random summing is possible between decaying nuclei. If they are not correlated, only random summing is possible. The discussion to follow includes all cases.



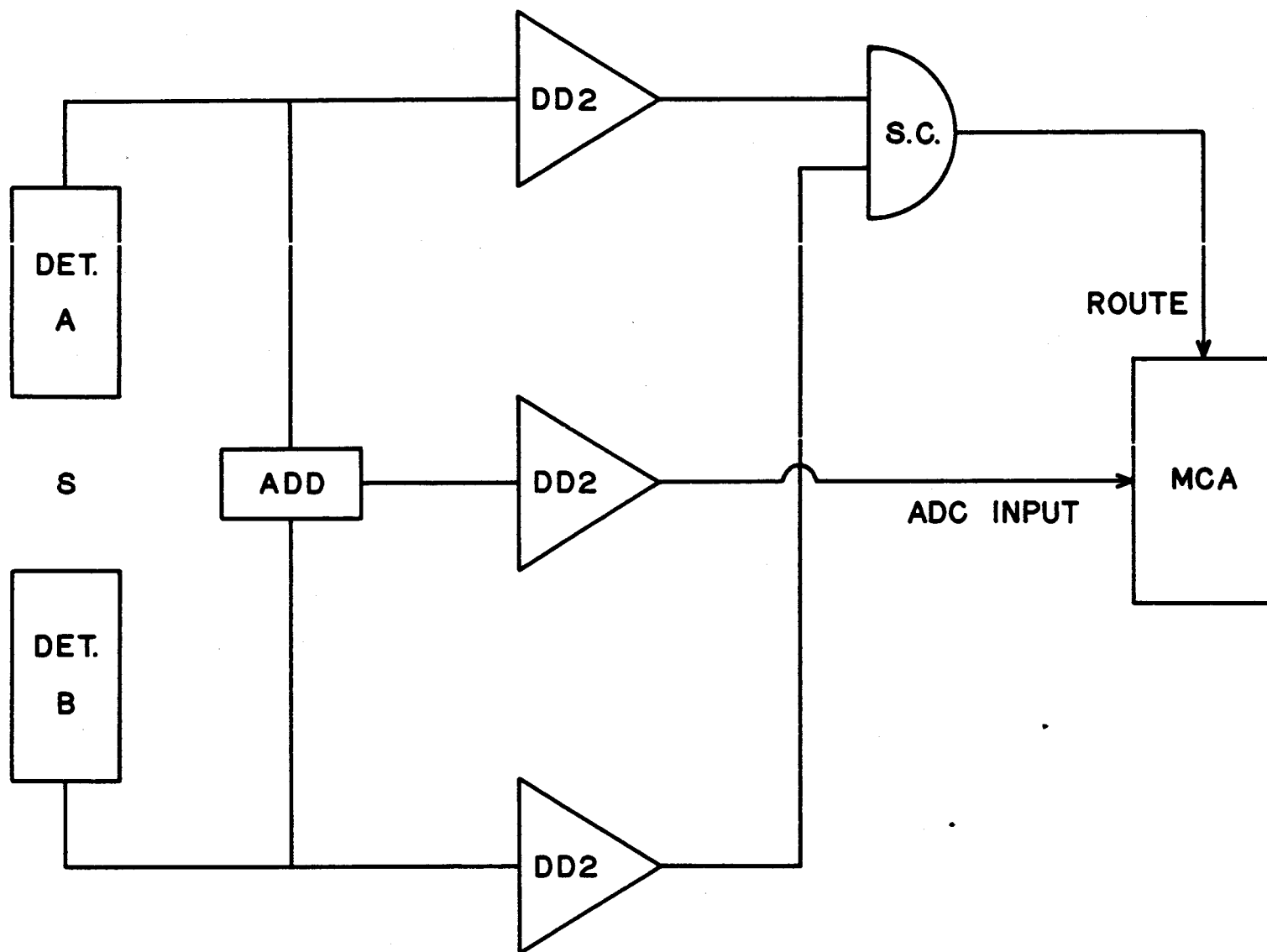
Two-Step Cascade    Three-Step Cascade

Figure 4

First, with two gamma rays only, X and Y, the system works as follows: If X goes in one crystal and Y goes into

---

\* The clipping time is the time constant of the amplifier output pulses.



SUM-COINCIDENCE SYSTEM

FIGURE 3

the other and are within coincidence timing resolution, then the sum pulse XY is routed into the MCA. If X and Y both enter the same crystal then the sum pulse XY is not routed but enters the normal MCA channels. As well, detectors A and B act as single crystals and their single spectra enter the MCA in the regular channel group. Thus, in the regular analyzer channels will be the sum spectrum plus the sum of two single spectra, viz:

$$(XY)_A + (XY)_B + X_A + X_B + Y_A + Y_B = 2(XY) + 2X + 2Y \quad \dots(2.5)$$

since there is no way to distinguish between detector A and detector B because they have the same gain and resolution. The routed spectrum will occur only when X and Y go in opposite directions. Thus it can consist only of:

$$X_A Y_B + X_B Y_A = 2(XY) \quad \dots(2.6)$$

By subtracting the routed spectrum from the regular spectrum, (channel by channel subtraction is permitted since no gain shift between the two spectra is possible) the resultant is just the sum of two single spectra, viz:

$$2XY + 2X + 2Y - [2(XY)] = 2X + 2Y = 2(X+Y) \quad \dots(2.7)$$

Secondly, with three gamma rays, X, Y, and Z, the two-crystal system produces the following results:

The normal MCA channels will contain

$$(XYZ)_A + (XYZ)_B + (XY)_A + (XZ)_A + (YZ)_A + (XY)_B + (XZ)_B + (YZ)_B \\ + X_A + Y_A + Z_A + X_B + Y_B + Z_B =$$

$$2(XYZ) + 2(XY) + 2(XZ) + 2(YZ) + 2X + 2Y + 2Z \quad \dots(2.8)$$

The routed MCA channels will contain

$$X_A Y_B + X_B Y_A + X_A Z_B + X_B Z_A + Y_A Z_B + Y_B Z_A + X_A (YZ)_B + X_B (YZ)_A$$

$$+Y_A(XZ)_B + Y_B(XZ)_A + Z_A(XY)_B + Z_B(XY)_A =$$

$$2(XY) + 2(XZ) + 2(YZ) + 6(XYZ) \quad \dots(2.9)$$

The resultant spectrum on subtraction of the summing effect will then be

$$2X + 2Y + 2Z - 4(XYZ) = 2(X+Y+Z) - 4(XYZ) \quad \dots(2.10)$$

which is just the sum of two single spectra again but now over-corrected for the triple-sum pulse. Since the probability of the triple sum is small compared to the double sum, it is felt that the over-correction by the subtraction of the routed spectrum from the combined spectrum to yield the single spectrum is negligible.

#### (b) Bremsstrahlung

A final contribution to the single spectrum is the detection of beta particles -- either directly or as Bremsstrahlung radiation. The electrons themselves are readily stopped by using an absorber in front of the NaI crystal. But in the process, the de-accelerating electrons emit Bremsstrahlung radiation. To keep this at a minimum, a one centimeter thick polyethylene disc was used as the absorber. The effective Z of polyethylene is low and this improves the ratio of radiationless energy dissipation to Bremsstrahlung radiation.

### 2.3 Pair Spectrometry

#### (a) The Spectrometer

The three-crystal pair spectrometer system used is shown in Figure 5. (F.C. is a fast coincidence circuit with a resolving time of  $2\tau = 60$  nsec.) Only the central

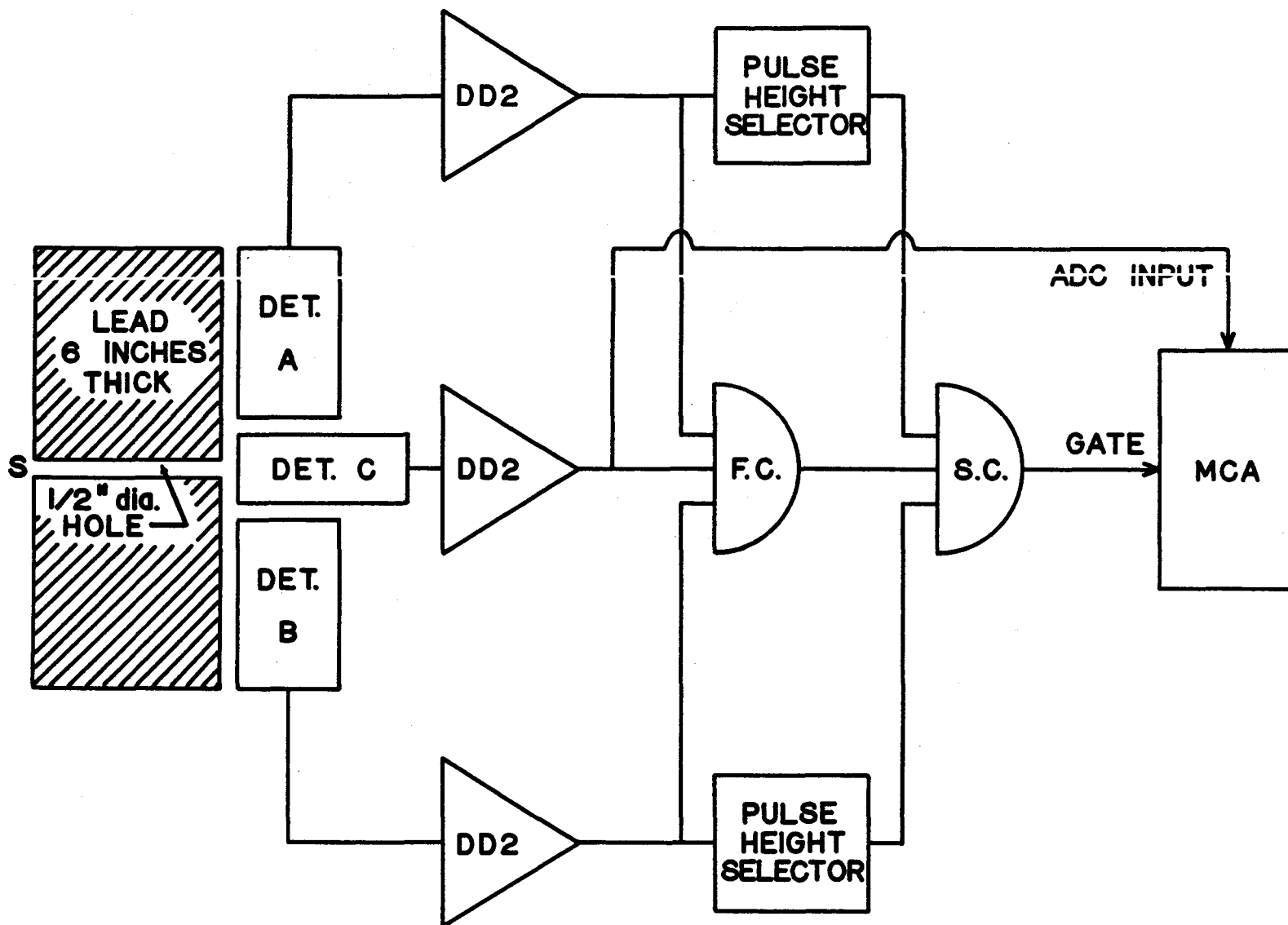


FIGURE 5

# THREE-CRYSTAL PAIR SPECTROMETER SYSTEM

crystal C ( $1" \times 1\text{-}1/2"d$ ) is exposed to gamma rays from the source. If the energy of the incident gamma ray exceeds that required to produce an electron-positron pair (1.022 MeV) then the remainder is carried off as kinetic energy of the two particles. The scintillator and photomultiplier convert this energy to a signal which can be amplified and recorded in the multichannel analyzer.

When the positron comes to rest, it combines with an electron and the resulting annihilation process produces two 511-keV gamma rays moving in opposite directions. The small dimensions of the central crystal enhance the possibility that neither of these annihilation gamma rays will interact with the crystal but will escape and be detected by the 3x3-inch side crystals A and B. By requiring that a triple coincidence among the three crystals is necessary before the centre crystal pulse is analyzed, most spurious and other undesirable pulses in the centre crystal can be eliminated. The energy of the gamma ray is then just 1.022 MeV plus that entering the multichannel analyzer.

A further refinement is the use of pulse-height selectors ensuring that the energy of the accepted gamma rays in the side crystals is indeed 511 keV. Without this improvement there is another interaction which will trigger all three detectors giving erroneous results. This is when one or both 511-keV annihilation gamma rays undergo Compton scattering within the central crystal and are detected by the side crystals as well, triggering the coincidence

circuitry. The signal sent by the centre crystal will then be increased by the amount of energy transmitted to the electrons by the scattering. By setting the side crystal pulse-height selectors so that they will accept only energies of about 511 keV, the forward scattered gamma rays, of lower energy, will necessarily be rejected.

Figure 6 shows this. In Figure 6 (a), the 2.76 MeV pair spectrum for  $\text{Na}^{24}$  using no pulse height selector on the side crystals has its high-energy edge distorted due to the energy added by the Compton scattered electrons to the original energy supplied by the electron-positron pair. In Figure 6(b), when narrow windows about 511 keV are used to screen out the forward scattered gamma rays, the analyzer was not allowed to see the incorrect higher energy pulses, thus removing the distortion in the spectrum.

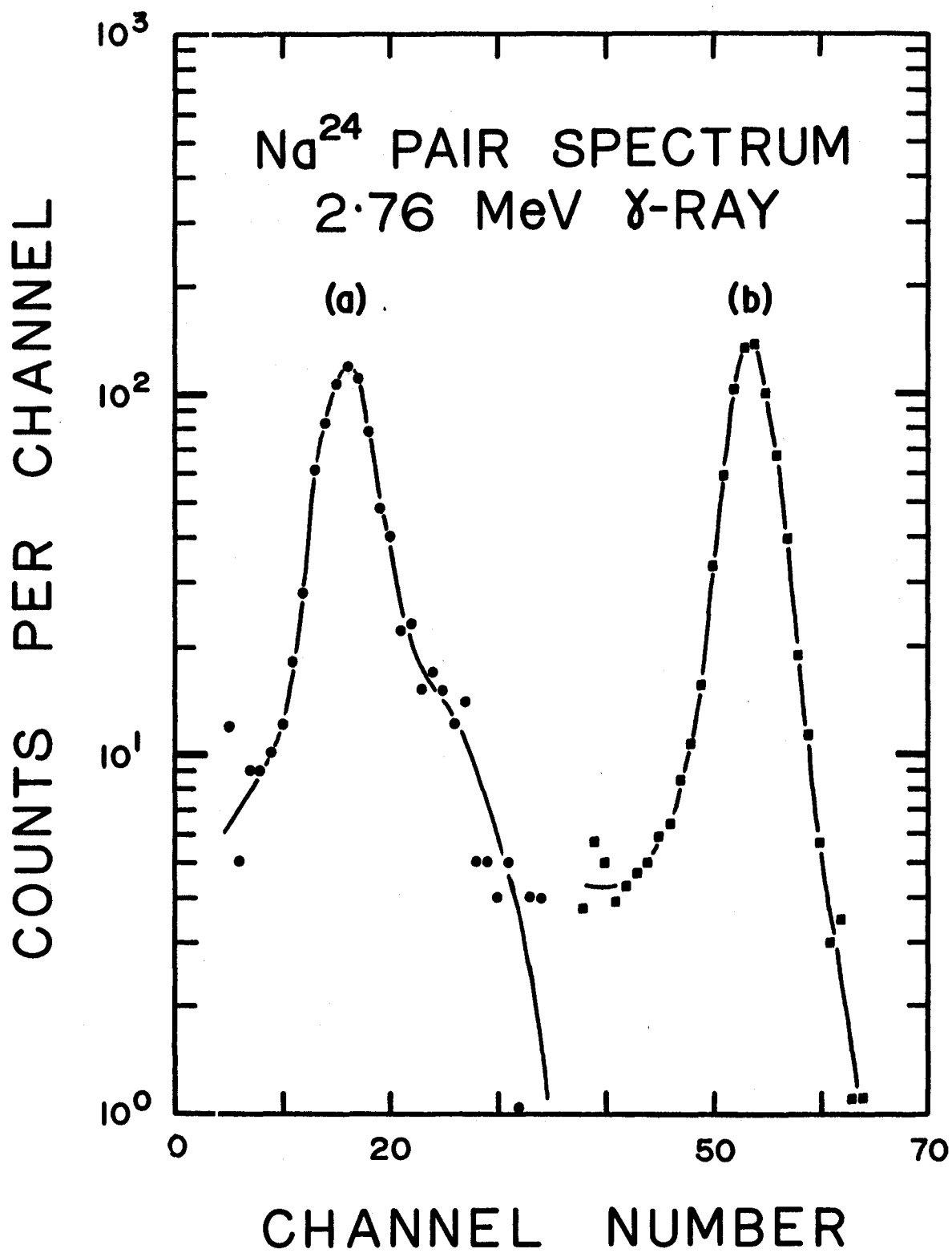
#### (b) Efficiency and Resolution

The relative efficiency of the pair spectrometer as a function of energy is assumed to follow the pair cross-section curve (3). For NaI, the pair-production linear attenuation coefficient  $K \text{ cm}^{-1}$  can be found knowing the same coefficient for lead  $K_{\text{Pb}}$  (4).

$$\left. \begin{aligned} K_{\text{Na}} &= K_{\text{Pb}} \left( \frac{\rho_{\text{Na}}}{11.35} \cdot \frac{207.2}{A_{\text{Na}}} \right) \left( \frac{Z_{\text{Na}}}{82} \right)^2 \\ K_{\text{I}} &= K_{\text{Pb}} \left( \frac{\rho_{\text{I}}}{11.35} \cdot \frac{207.2}{A_{\text{I}}} \right) \left( \frac{Z_{\text{I}}}{82} \right)^2 \end{aligned} \right\} \dots (2.11)$$

$$\text{and } K = K_{\text{I}} \left[ 1 + \frac{N_{\text{Na}}}{N_{\text{I}}} \left( \frac{Z_{\text{Na}}}{Z_{\text{I}}} \right)^2 \right] \dots (2.12)$$

FIGURE 6



where  $\rho$  is the density (11.35 g/cm<sup>3</sup> for Pb), A is the atomic weight (207.2 for Pb), Z is the atomic number (82 for Pb), and N is the number of atoms/cm<sup>3</sup> of an element in the absorber. The pair cross-section is then given by

$$\sigma_{pp}(\text{NaI}) = \frac{K}{\rho_{\text{NaI}}} = 0.084 K_{\text{Pb}} \text{ cm}^2/\text{g} . \quad \dots(2.13)$$

Figure 7 is a plot of the pair-production linear attenuation coefficient  $K_{\text{Pb}}$  as a function of energy (5).

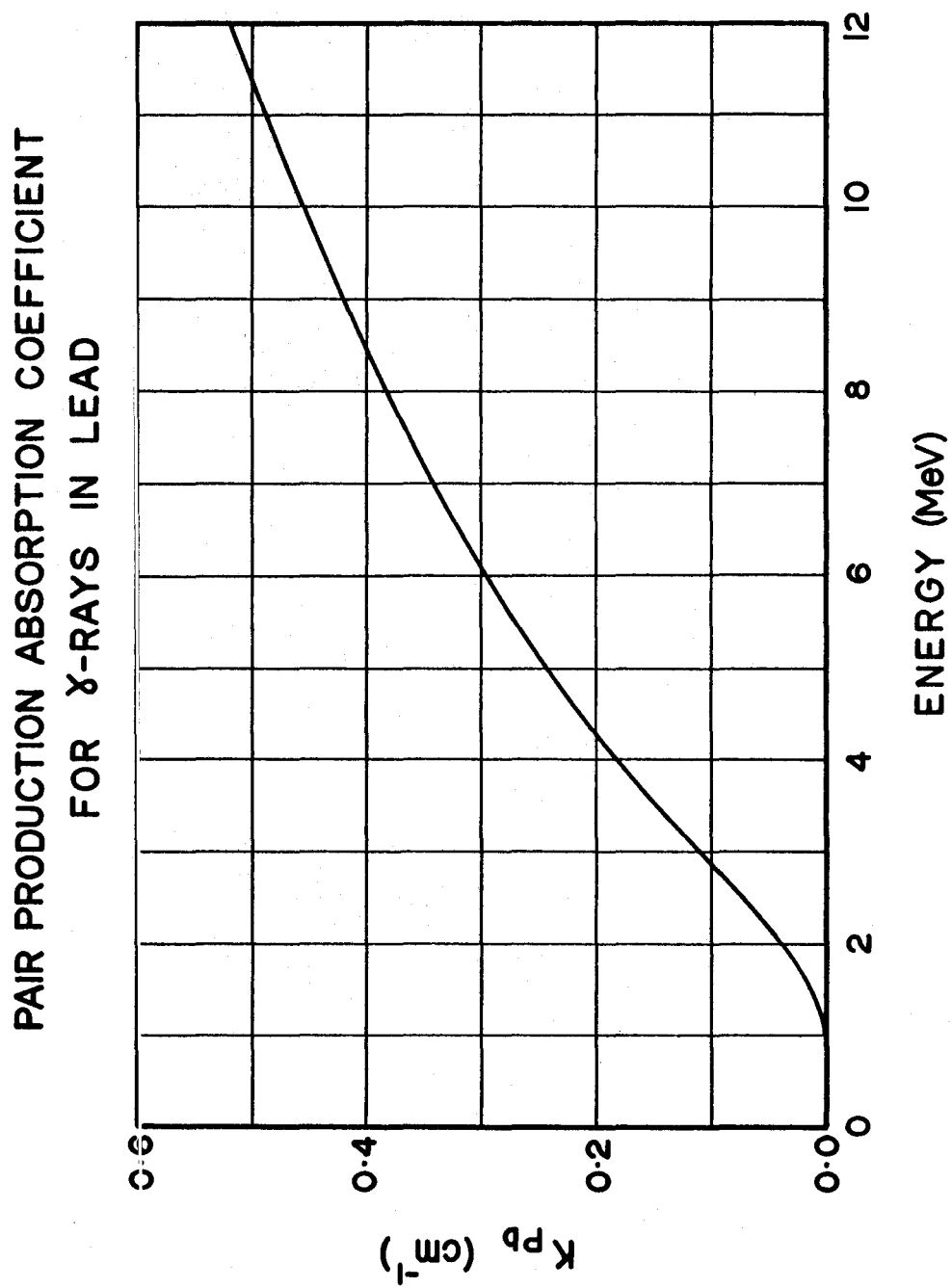
In the pair spectrometer, the energy analyzed in the crystal is reduced by 1.022 MeV hence the resolution of the spectrometer will be characterized by that for a gamma ray of energy  $E_\gamma - 1.022$  MeV rather than of energy  $E_\gamma$ . The absolute width of a spectral line obtained from a scintillation crystal increases as the energy deposited in the crystal increases. As a result, for the same crystal, the uncertainty in the value of energy  $E_\gamma - 1.022$  will be less than that for energy  $E_\gamma$ . Then the actual energy value obtained from the pair spectrometer by adding 1.022 MeV will be more reliable than if it had been obtained directly.

Specifically, photopeak resolution (width at one-half maximum) for a single crystal spectrum is  $\Delta E_s/E_\gamma$ . Using the three-crystal pair spectrometer system the effective resolution becomes  $\Delta E_p/(E_\gamma - 1.022)$ . Above about two MeV  $\Delta E_p \approx \Delta E_s$  and hence the pair spectrometer has improved the resolution by a factor of approximately

$$\frac{\Delta E_p}{E_\gamma - 1.022} \bigg/ \frac{\Delta E_s}{E_\gamma} = \frac{E_\gamma}{E_\gamma - 1.022} . \quad \dots(2.14)$$

For a two MeV gamma ray this represents a doubling of the resolution.

FIGURE 7



## 2.4 Two-Dimensional Coincidence Spectrometry

One-dimensional pulse-height analyzers for use in time correlation studies have been of great assistance in constructing decay schemes of radioisotopes. Such an instrument is shown in Figure 8. Ideally, only the gamma rays in coincidence with the gamma ray of the energy selected by the pulse-height selector will be recorded in the multi-channel analyzer. By altering the window of the pulse-height selector to only include each of the gamma rays observed in the single spectrum one at a time, a series of coincident gamma spectra are obtained which when analyzed generally yield a unique decay scheme.

But the window energy selected not only contains the photopeak of the gamma ray desired but also the Compton tails of higher energy gamma rays. These higher energy gamma rays have a coincidence spectrum of their own and these will contaminate the spectrum desired. The one-dimensional system gives no information on this Compton interference. Also the one-dimensional method is cumbersome when an isotope with a complicated decay scheme is under observation. In this case a large number of independent coincidence runs would have to be made and this would be extremely time consuming since the coincidence counting rate would be very much lower than singles. For shorter-lived isotopes this could involve preparation of numerous samples and normalization of the resulting data.

Using a two-dimensional instrument, all coincidences

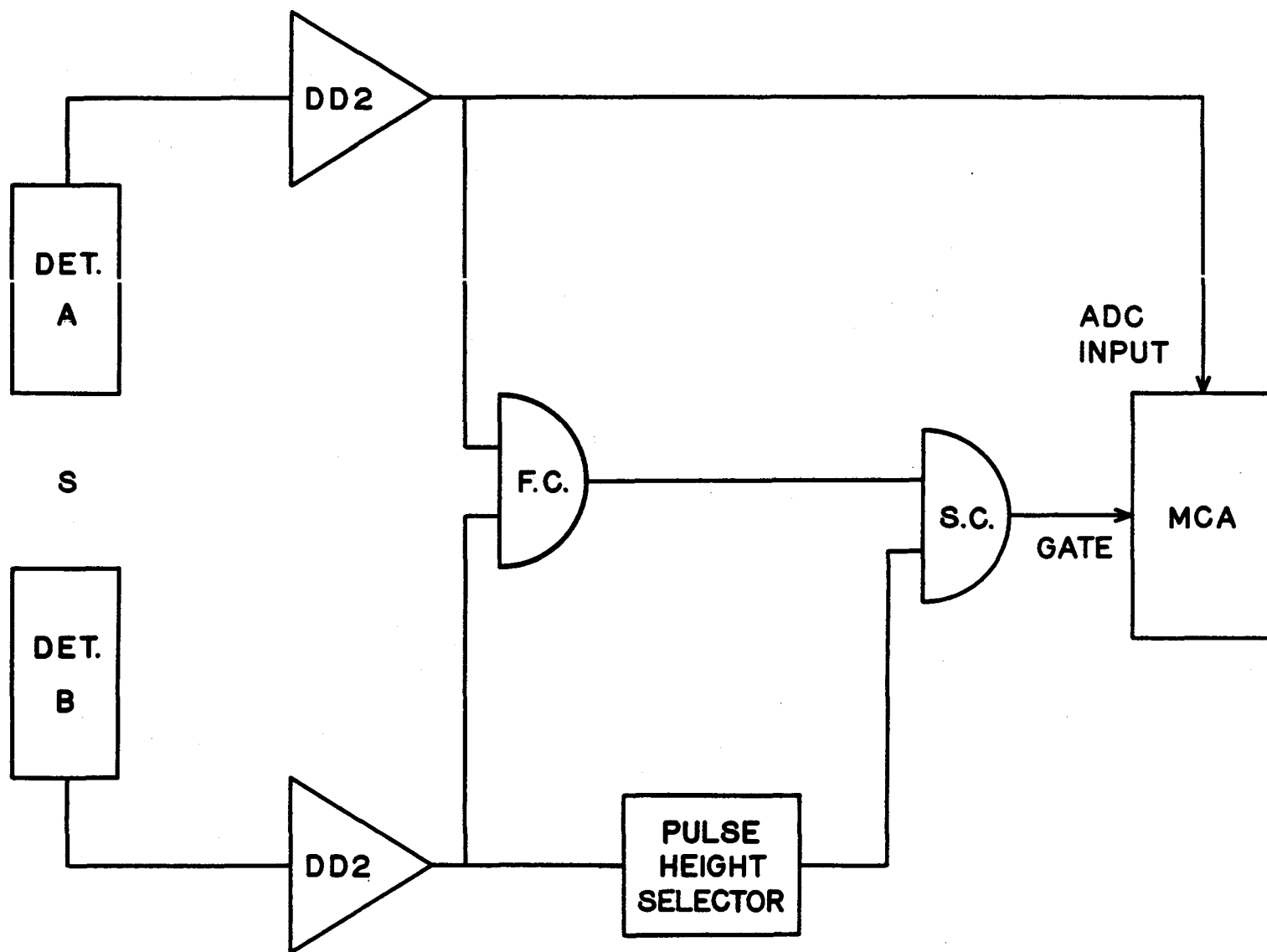


FIGURE 8

# ONE-DIMENSIONAL COINCIDENCE SYSTEM

with all window energies can be recorded simultaneously. Not only does this produce all the coincidence spectra for all the gamma rays involved but also it traces out the Compton interference in each by recording the Compton coincidence spectra in an energy region where only the Compton tail is present.

The instrument is simply an extension of the one-dimensional system. In principle, a series of pulse-height selectors covering the desired energy range each gate a different portion of the MCA. Consider the decay of  $\text{Sc}^{46}$  for example (see Figure 9). Assume at first that the single crystal response is ideal - that is, that the single spectrum is composed of two delta functions. In Figure 10 the block of 36 squares represents the MCA memory readout where  $n_{ij}$  is the number of counts in row  $i$ , column  $j$ . And each row (column) is the part of the memory readout which has responded to the windows  $w_1, w_2, \dots, w_6$  ( $v_1, v_2, \dots, v_6$ ). Thus each row (column) represents a single coincidence spectrum as would be produced by the one-dimensional instrument. The energies covered by the sets of windows  $w_i$  and  $v_j$  are indicated by the single spectrum of  $\text{Sc}^{46}$  shown on the sides.

For example, since  $w_3$  includes a part of the spectrum where there is no gamma radiation, then it should have no coincidence spectrum and  $n_{3j} = 0$  for all  $j$ . But  $w_4$  includes the 887-keV gamma ray and its coincidence spectrum should contain the 1119-keV gamma ray. Window  $v_6$  covers this energy range so  $n_{4j} = 0$  for all  $j$  except  $j = 6$ . Similarly  $n_{55}$  will

FIGURE 9

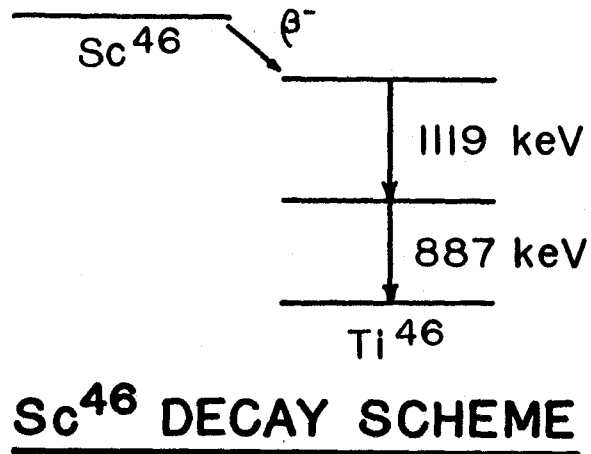
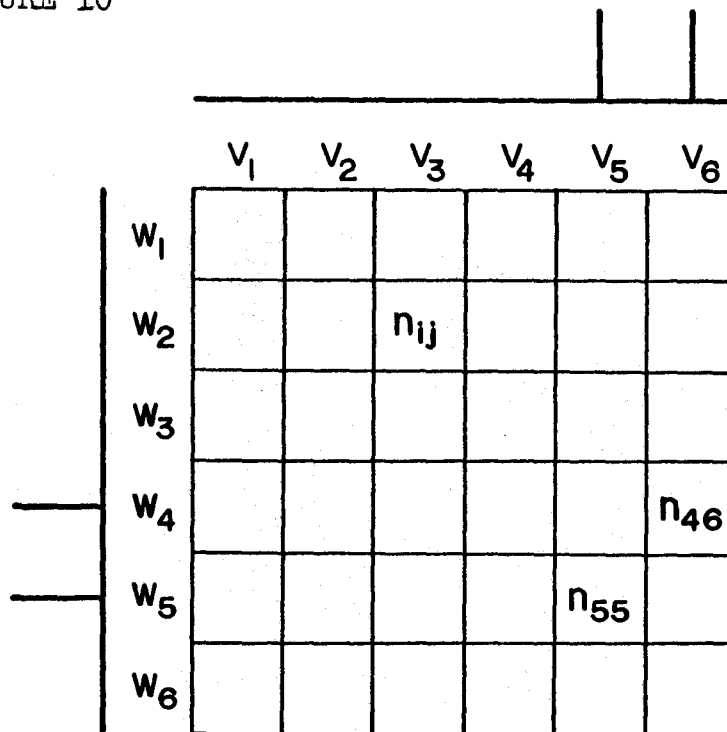


FIGURE 10

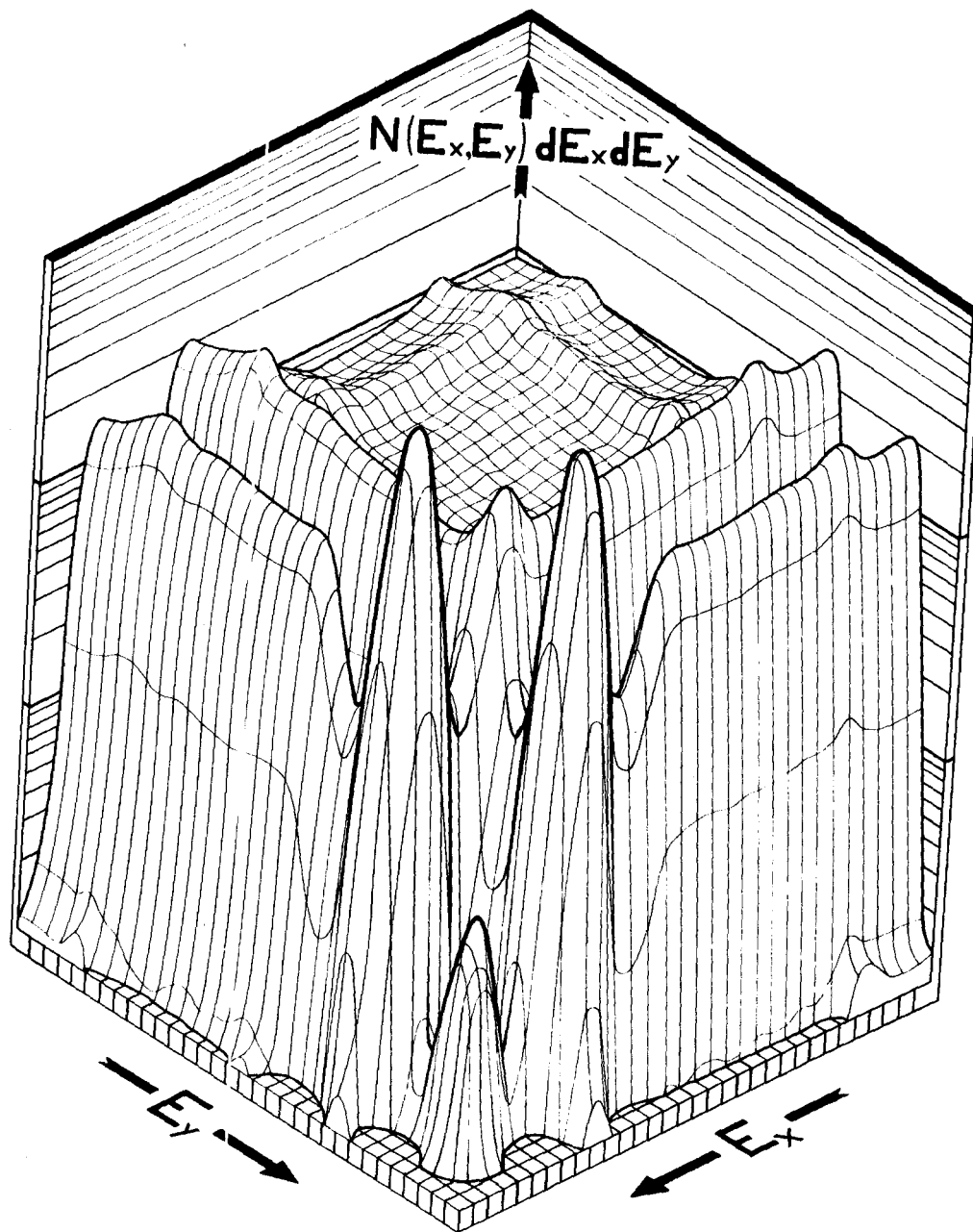


**IDEAL TWO-DIMENSIONAL COINCIDENCE  
ARRAY FOR  $Sc^{46}$**

be non-zero. Looking at the complete array in this fashion, the ideal case for  $\text{Sc}^{46}$  would in fact have only counts  $n_{55}$  and  $n_{46}$  showing. This is true provided we ignore the possibility of chance events, when gamma rays from different nuclei gate the coincidence circuit. This leads to a few counts  $n_{45}$  and  $n_{56}$ . Also  $n_{55}$  and  $n_{46}$  would partly be made up from chance. So once the energy scales have been established a quick look at the array for the high count regions readily establishes the coincident gamma rays. If the energy scales are the same, the readout will be symmetrical.

A 1024-channel two-dimensional analyzer was used in this study. The arrays available with this instrument were  $8 \times 128$ ,  $16 \times 64$ , and  $32 \times 32$  channels in each dimension. Using the  $32 \times 32$  array form, the two-dimensional coincidence spectrum of  $\text{Sc}^{46}$  was measured and the results have been plotted in the isometric drawing Figure 11. Here it is readily noted that the majority of  $n_{ij} \neq 0$  and the coincident photopeaks are not delta functions. This is, of course, because the crystal response is not ideal as at first assumed. However the coincident photopeaks are readily discernible as they lie a factor of ten or more above the Compton peak, chance peak, and other coincident points.

FIGURE 11

TWO-DIMENSIONAL COINCIDENCE SPECTRUM OF  $\text{Sc}^{46}$

## CHAPTER III

### Br<sup>82</sup> DECAY SCHEME

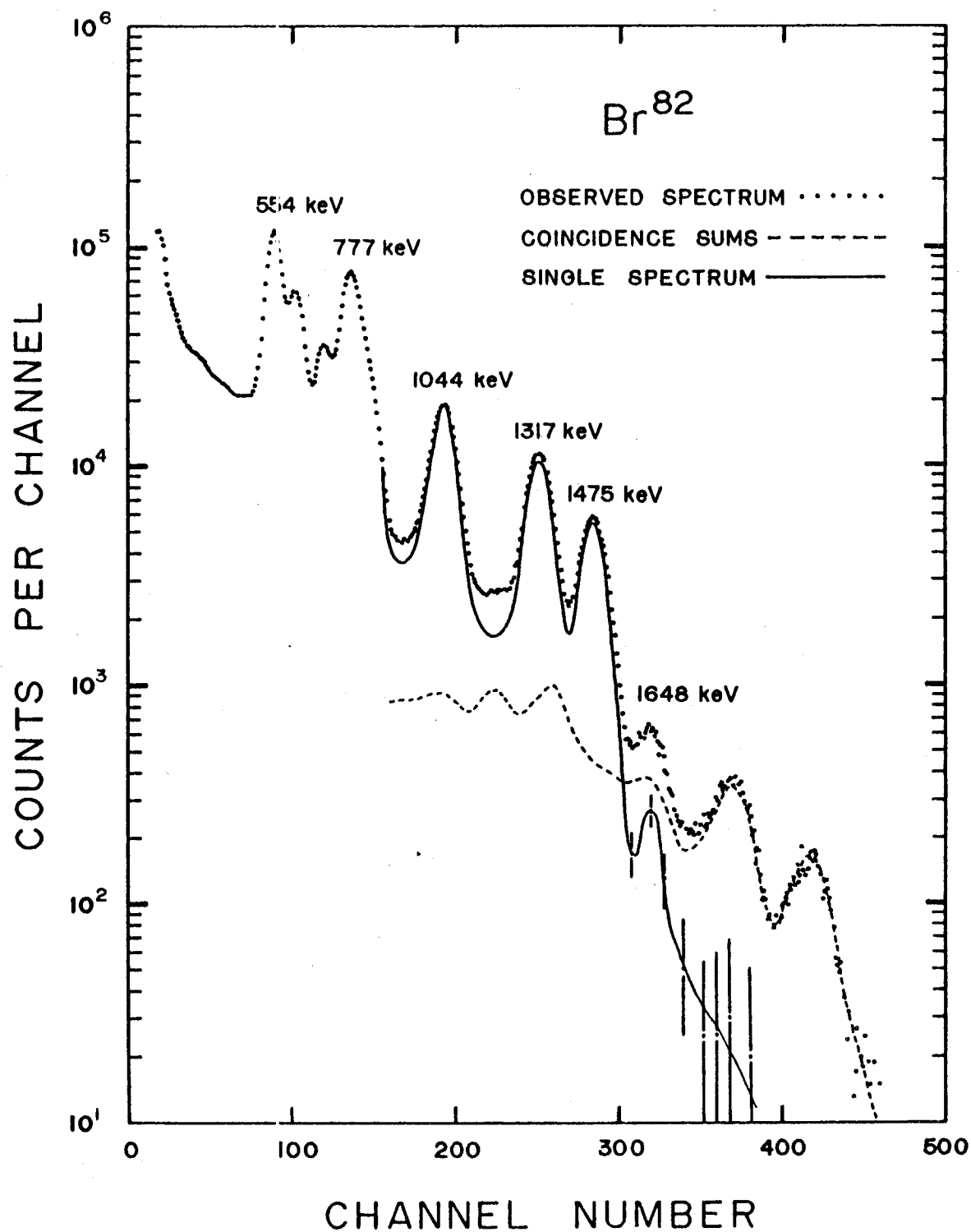
#### 3.1 Single Spectrum

The single-crystal gamma-ray spectrum was observed with an unshielded 3x3-inch NaI(Tl) crystal integrally mounted on a DuMont 6363 photomultiplier. A polyethylene beta-ray absorber was attached to the crystal face. The spectrum was recorded in a 1024-channel Nuclear Data pulse-height analyzer after amplification in a DD2 linear amplifier.

The spectrum obtained with the source at 10 cm. and corrected for room background is shown in Figure 12. To correct for the contribution from coincidence and random summing, the analyzer was operated in the split memory mode using two groups of 512 channels each as outlined in Chapter II, Section 2(a). The associated sum-coincidence contribution and the corrected single spectrum are also indicated in Figure 12.

The sum coincidence completely accounts for the highest energy peak in the observed singles and also for the second highest energy peak (about 1900 keV) within statistics. A third peak at energy about 1648 keV can not

FIGURE 12



be accounted for in terms of coincidence or random summing. As the resultant single spectrum indicates, the 1648-keV energy peak appears to correspond to an actual gamma ray. For energies below this to 500 keV the single spectrum is identical to that found by earlier experimenters (1).

### 3.2 Pair Spectrum

Figure 13 is a typical pair spectrum for  $\text{Br}^{82}$  using narrow windows at the 511-keV gate as suggested in Chapter II, Section 3(a). The 1317- and 1475-keV lines are very prominent and the existence of an even higher energy line is obvious. Its energy is about 1648 keV. Above this is a continuum consisting of a few counts per channel. Coincidence summing can not account for this but random summing probably does. However, if a gamma ray of energy 1900 keV does exist, on the basis of the number of counts in that region of the pair spectrum, its intensity must be less than 5% of the 1648-keV gamma ray.

### 3.3 Coincidence Spectrum

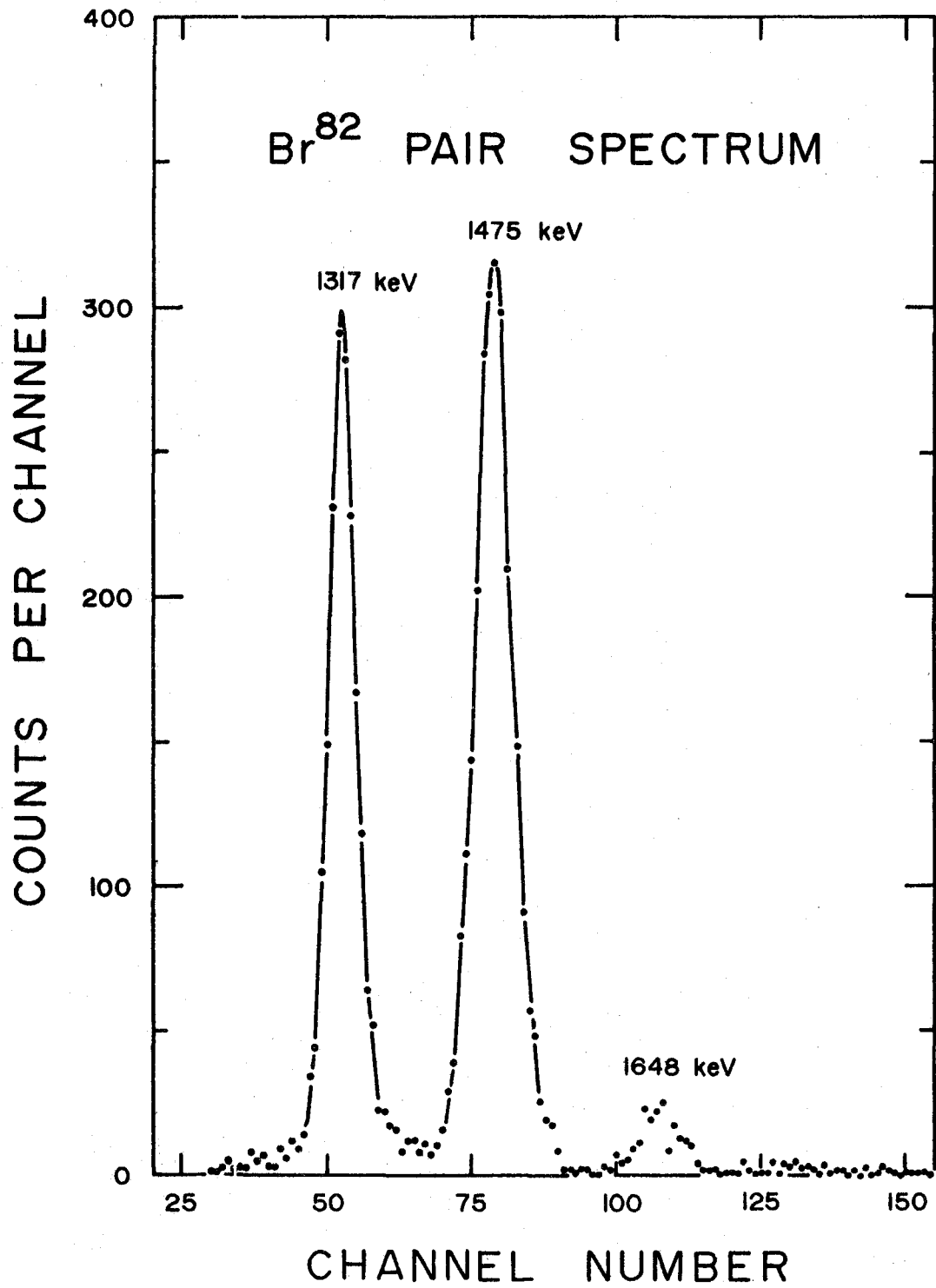
The coincidence spectra were taken with the crystals at  $180^\circ$  mounted on arms 7" above a  $3/4$ " channel aluminum track. This was placed in the middle of the room to minimize any backscattering. The  $\text{Br}^{82}$  sample was sandwiched between celluloid tape and mounted on an anti-Compton shield.\* Arrays of 16x64 and 32x32 were used to produce the best results.

With an energy range of 1550 to 1750 keV for the

---

\* An anti-Compton shield prevents one detector from seeing the Compton scattered radiation from the other.

FIGURE 13



16 dimension and 0 to 800 keV for the 64 dimension, the gamma spectrum in coincidence with the 1648-keV line was formed. This is shown in Figure 14 which indicates that gamma rays of energy 777 and about 220 keV are coincident with it. It also appears as if the 554-keV line is coincident but this would seem impossible on looking at the decay scheme if the 1648-777 coincidence is true. The 554 line appears because of interference from the 1475-554 and 1475-619 keV correlations. To verify this, Figure 15 shows slices in the 16 channel dimension at 220, 554, and 777 keV. The 220- and 777-keV coincidence spectra clearly show the 1648-keV line while the 554-keV spectrum shows no indication of a peak in this region. The exponential drop-off observed in this spectrum is attributable to random and coincidence summing. The resolution of the 1648-keV coincidence spectrum from the above mentioned interference can be achieved if one resolves each row of 16 channels into a 1648-keV peak, a 1475-keV peak, and an exponential term.

Using the method of least squares, the 1024 channels of data were analyzed 16 channels at a time and resolved into three components:  $a_i(1648)$ ,  $b_i(1475)$ , and  $c_i(\exp)$ . The resulting 64 values for  $a_i$  give the coincidence spectrum for the 1648-keV line component. This has been plotted as well in Figure 14, indicating that the 1648-keV transition is in coincidence with the 220- and 777-keV transitions.

Two 32x32 array arrangements were run covering the

FIGURE 14

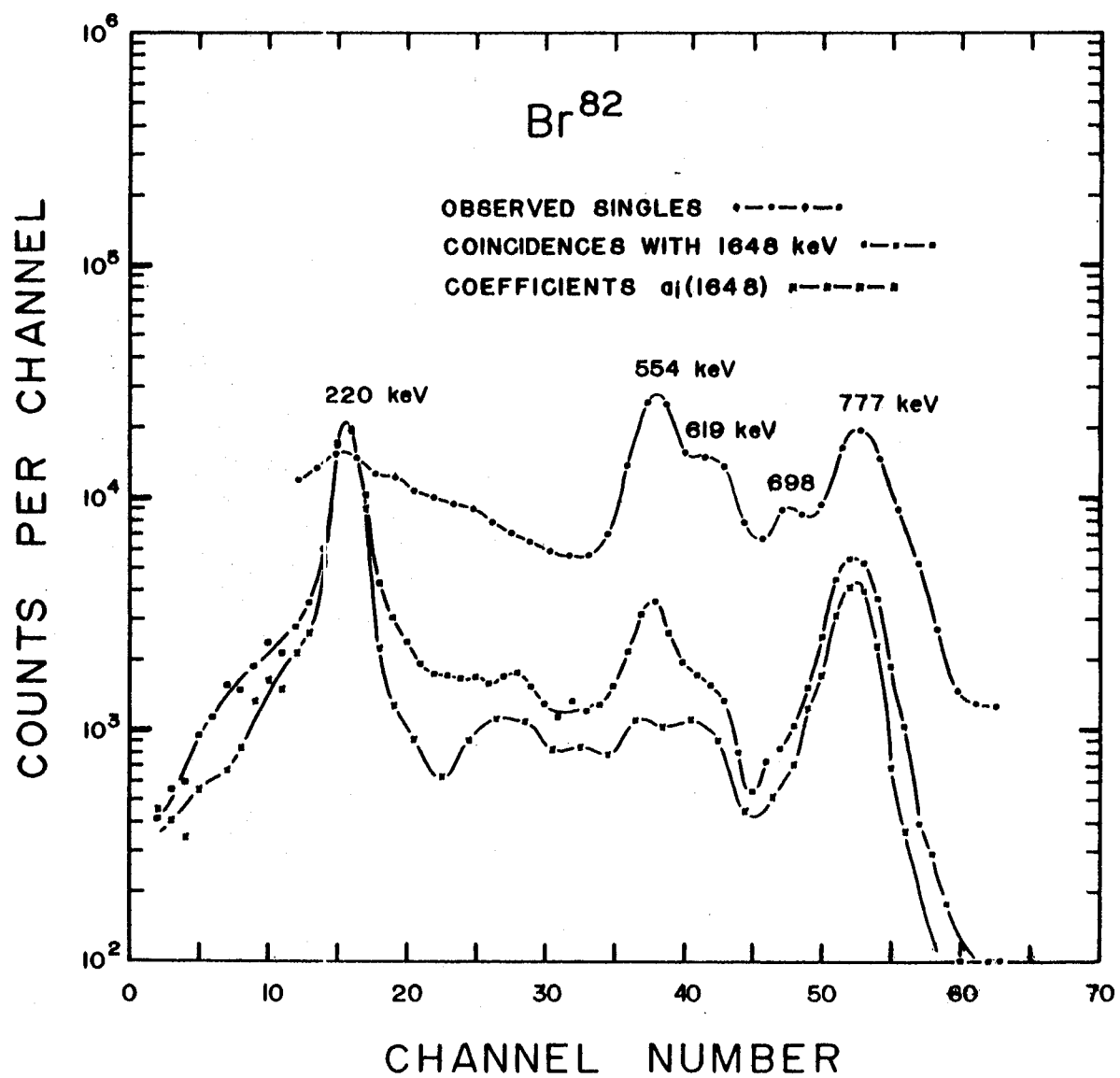
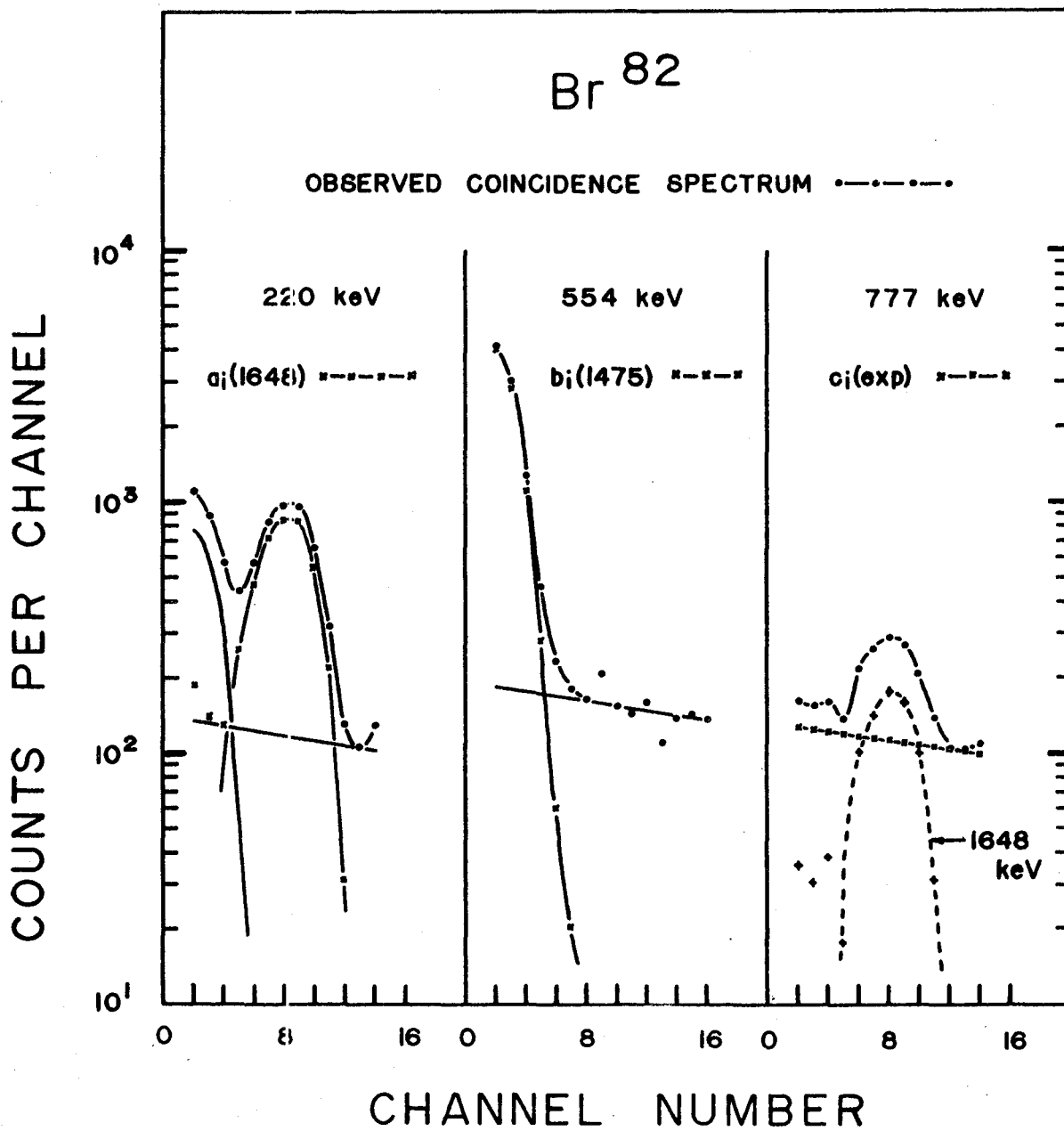


FIGURE 15



energy range from 0 to 900 keV coincident with 0 to 1800 keV. The results verified the decay scheme presented in the Nuclear Data Cards (1) except for the 250-350-keV cascade.

### 3.4 Revised Decay Scheme

#### (a) Energies

The gamma-ray energies between 500 and 1500 keV as recorded on the decay scheme in the Nuclear Data Cards (1) were used to obtain the energies of the 220- and 1648-keV lines by extrapolation from the various spectra, correcting for the non-linearity of the NaI crystal. The results are tabulated below in Table I.

The transitions previously reported at 250 and 350 keV were not found.

TABLE I

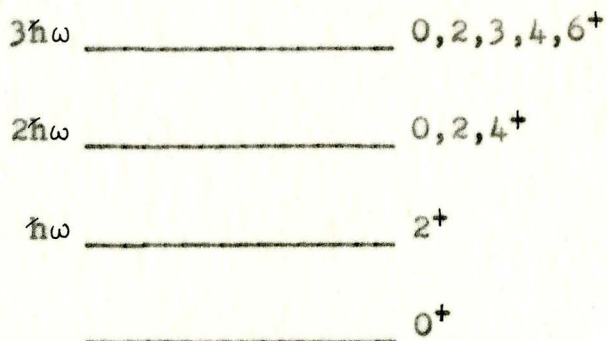
New Gamma-Ray Energies for  $\text{Br}^{82}$

$\gamma$ -Ray	Type of Spectrum	Energy Obtained	Average with Standard Deviation
220	16x64 16x64 32x32	219 214 227	$220 \pm 7$ keV
1648	Single Pair Pair	1646 1647 1651	$1648 \pm 3$ keV
Total Energy			$1868 \pm 10$ keV

The total energy recorded in Table I agrees with the 1871 keV required to fit between the 2648- and 777-keV levels in  $\text{Kr}^{82}$ . The cascade can then follow the decay pattern 220-1648-777 or 1648-220-777. This sets up a new energy level in  $\text{Kr}^{82}$  at 2426 or 997 keV respectively.

Examination of the neutron and proton pairing energies compiled by Dewdney (6) indicate that the first particle state would be at approximately 2400 keV for this mass. Therefore the states below this energy are collective in nature.

The  ${}_{36}\text{Kr}_{46}^{82}$  nuclide is even-even with a neutron number near the 50 shell. This suggests that  $\text{Kr}^{82}$  will be nearly spherical in shape and indicates it will exhibit vibrational rather than rotational properties. Assuming the vibrational oscillations are small, they can be approximated by simple harmonic motion. A solution of the Schrodinger wave equation using the harmonic oscillator potential well yields a series of possible energy levels separated in energy of an amount  $\hbar\omega$  where  $\omega$  = classical vibration frequency as indicated in Figure 16. The lowest mode of



Quadrupole Vibrational Spectrum for  
Even-Even Nuclei with Spherical Equilibrium Shape

Figure 16

deformation of this system is of quadrupole type. Hence the first excited state has a total angular momentum of two units and positive parity. The second states contain two quanta of excitation and the total angular momentum values may be obtained by coupling the two quanta, each having an angular momentum of two units. However, the model permits only the symmetric combinations  $J = 0, 2, 4$  with positive parity. The degeneracy of the level is a result of the use of the ideal simple harmonic potential. In actual fact the levels are separated in energy (7).

Examining the  $\text{Kr}^{82}$  energy-level scheme as shown in Figure 1 using the above background, it can be seen that the 777- and 1475-keV levels probably correspond to the first two excited harmonic oscillator levels with spins  $2^+$ . The proposed 997-keV level then could be either the  $J = 0^+$  or  $4^+$  level. The  $J = 0^+$  level can be excluded because this would mean the transition from 2648 keV to the proposed level would be an  $M4$  transition which has a very small transition probability and unlikely to compete with the other gamma rays leaving the level.

Assume that the proposed 997-keV level is the  $4^+$ . There is a possibility that beta decay could occur to the level from  $\text{Br}^{82}$ . This would be a first-forbidden decay. A  $\log_{10} f$  of 9 is a typical maximum for first-forbidden decay in this mass region (8) and using the  $\log_{10} f$  values from Evans (9) it follows that :

beta end point energy  $E_{\max} = 2.1 \text{ MeV}$ ,

$$\log_{10} f [Z=36, E=2.1] = 2.5,$$

and  $\log_{10} t_1 = \log_{10} f - \log_{10} f = 9 - 2.5 = 6.5$ ;

therefore  $t_1 = 3.2 \times 10^6$  seconds

and since total half life  $t = 36 \text{ hr.} = 1.3 \times 10^5 \text{ sec.}$ ,

the branching ratio would be:

$$\frac{1/3.2 \times 10^6}{1/1.3 \times 10^5} = \frac{1.3}{32} = 4\% .$$

However, an upper limit for higher energy beta-ray groups has been reported to be less than 0.6% (10). Thus an energy level at 997 keV is inconsistent with beta-ray measurements. Furthermore, other even-even nuclides in this mass region do not have low-lying second energy levels.

It is more realistic then to have an energy level at 2426 keV. The order of the gamma cascade is then 220-1648-777. This would lead to the low intensity observed for this branch since the 220-keV transition would be in competition with the 554- and 827-keV transitions. The insertion of this level and the removal of the 250- and 350-keV gamma rays leads to the revised decay scheme show in Figure 17.

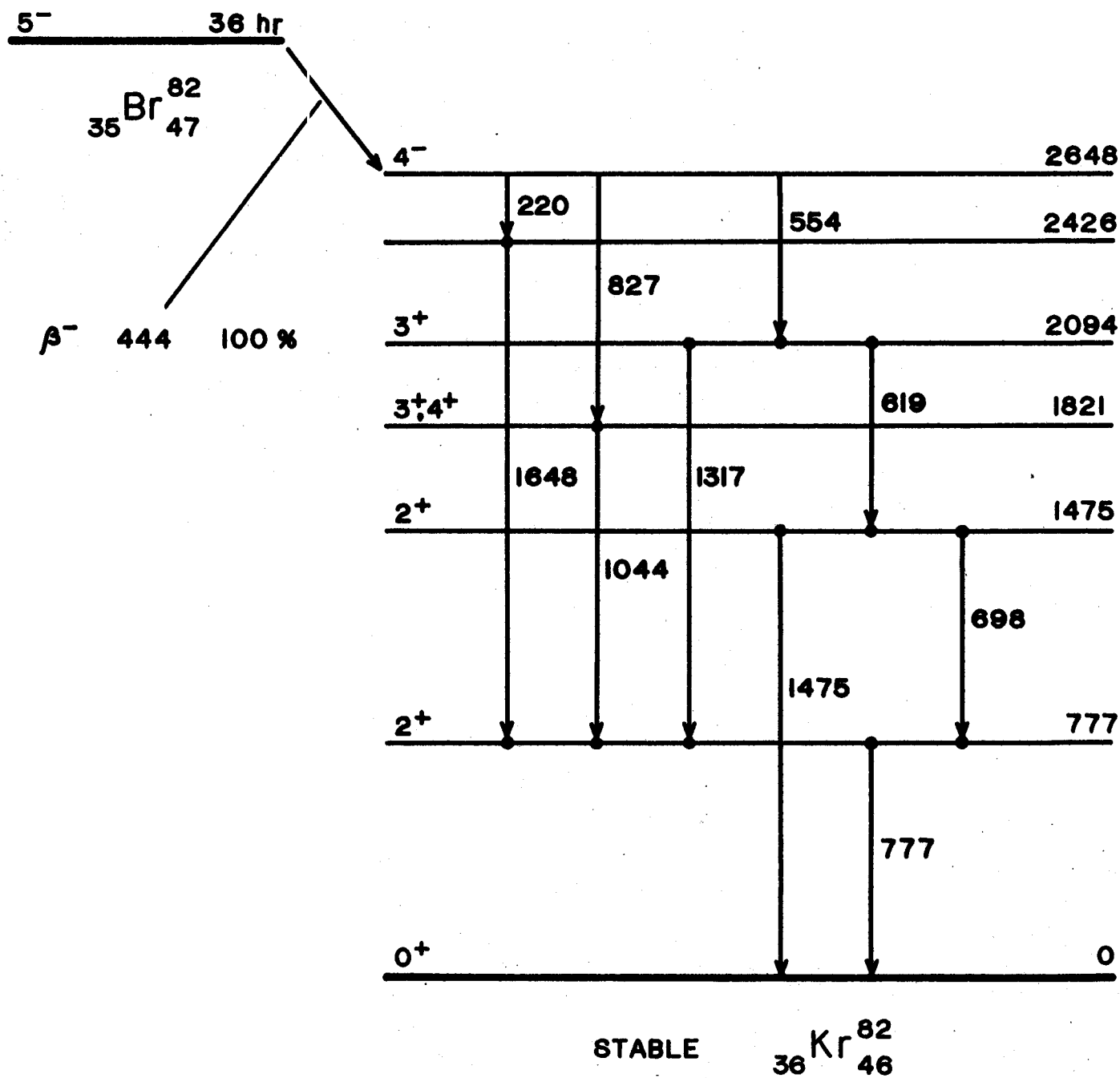
#### (b) Intensities

The relative intensities of the 1044-, 1317-, 1475-, 1648-, and 1900 (if it exists)-keV gamma rays were calculated from the single and pair spectra. The results are indicated in Table II below.

The intensities of all the gamma rays as obtained from a reduction of the coincidence data is tabulated in a

# REVISED $\text{Br}^{82}$ DECAY SCHEME

(ALL ENERGIES IN keV)



later section.

TABLE II  
Some Gamma-Ray Intensities for Br<sup>82</sup>

$\gamma$ -Ray	Relative Intensity Singles	Relative Intensity Pair	Average Value	Intensity Based on 1475 = 20 or 777 = 100
1044	8.5			38 <sup>+</sup> 10%
1317	6.5	6.5 *	6.5	29
1475	4.8	4.3	4.5	20
1648	0.2	0.2	0.2	~ 1
1900	< 0.05	< 0.01	< 0.01	< 0.05

\* Normalized to the Singles value

## CHAPTER IV

### REGRESSION ANALYSIS

#### 4.1 Reduction of Coincidence Surface

##### (a) Outline

The coincidence surface is obtained in the form  $S(x,y)$  where  $x$  and  $y$  are the digitized coordinates and  $S(x,y)$  is the number of events at  $(x,y)$ . The surface corresponding to a coincident pair of gamma rays  $\gamma_i$  and  $\gamma_j$  is given by  $X_i(x)Y_j(y)$  where  $X_i$  and  $Y_j$  are the response functions.

The equation for the model is of the form

$$S(x,y) = \sum_{i,j=1}^n a_{ij} X_i(x) Y_j(y) , \quad \dots(4.1)$$

where  $a_{ij}$  are the intensity correlation coefficients.

The model equation can be reduced to a set of coupled equations

$$S(x,y) = \sum_{i=1}^n a_i(y) X_i(x) \quad \dots(4.2a)$$

and 
$$a_i(y) = \sum_{j=1}^n a_{ij} Y_j(y) . \quad \dots(4.2b)$$

Now consider whether a regression analysis of the coupled equations 4.2 can be carried out in such a way as to lead

to the same results as an analysis of 4.1 .

(b) Analysis of Coupled Equations

From the least squares condition and weighting with the variance  $S(x,y)$ , in 4.2a,

$$\sum_{x=1}^N \frac{1}{S(x,y)} \left[ S(x,y) - \sum_{i=1}^n a_i(y) X_i(x) \right]^2 \text{ must be a minimum.}$$

For a minimum, the partial derivative with respect to  $a_i(y)$  equals zero. Therefore we get

$$\sum_{x=1}^N \left[ S(x,y) - \sum_{i=1}^n a_i(y) X_i(x) \right] \frac{X_k(x)}{S(x,y)} = 0 \quad \dots(4.3)$$

where  $i = 1, 2, \dots, n$  } number of lines in X direction  
 $k = 1, 2, \dots, n$  }  
 $x = 1, 2, \dots, N$  number of channels in X direction.

These equations 4.3 are solved for each  $y = 1, 2, \dots, N$  to give the  $n \times N$  set  $a_i(y)$ .

Similarly, performing the least squares condition on 4.2b yields

$$\sum_{y=1}^N w_y \left[ a_i(y) - \sum_{j=1}^n a_{ij} Y_j(y) \right] Y_l(y) = 0 \quad \dots(4.4)$$

where  $j = 1, 2, \dots, n$  } number of lines in Y direction  
 $l = 1, 2, \dots, n$  }  
 $y = 1, 2, \dots, N$  number of channels in Y direction  
 $w_y$  = weight function.

From 4.4,

$$\sum_{y=1}^N w_y Y_1(y) a_i(y) = \sum_{y=1}^N w_y Y_1(y) \sum_{j=1}^n a_{ij} Y_j(y) \quad \dots (4.5)$$

Multiply each side of 4.3 by  $w_y Y_1(y)$  and sum over  $y$  to give

$$\sum_{y=1}^N w_y Y_1(y) \left[ \sum_{x=1}^N \left[ S(x,y) - \sum_{i=1}^n a_i(y) X_i(x) \right] \frac{X_k(x)}{S(x,y)} \right] = 0 \quad .$$

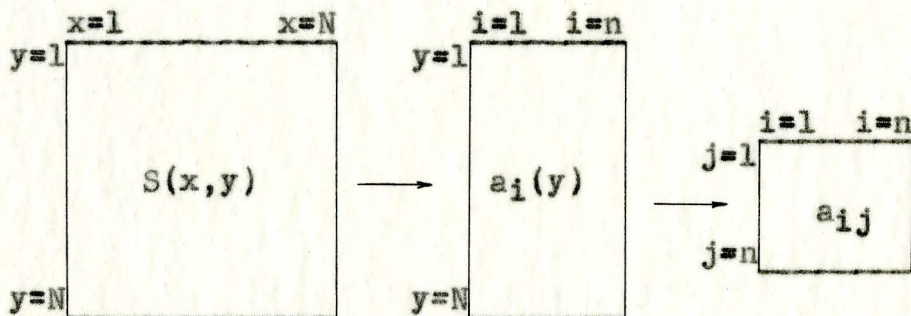
Simplifying,

$$\sum_{y=1}^N w_y Y_1(y) \left[ \sum_{x=1}^N S(x,y) \frac{X_k(x)}{S(x,y)} \right] - \sum_{x=1}^N \sum_{i=1}^n \left[ \sum_{y=1}^N w_y Y_1(y) a_i(y) \right] \frac{X_i(x) X_k(x)}{S(x,y)}$$

Substituting from 4.5 and simplifying yields

$$\sum_{y=1}^N \sum_{x=1}^N \left( w_y / S(x,y) \right) \left[ S(x,y) - \sum_{i=1}^n \sum_{j=1}^n a_{ij} Y_j(y) X_i(x) \right] Y_1(y) X_k(x) = 0 \dots (4)$$

This two step regression analysis is shown schematically in Figure 18.



Reduction of Coincidence Surface by Regression Analysis

Figure 18

### (c) Analysis of Original Model Equation

From the least squares condition on 4.1 we get

$$\sum_{x=1}^N \sum_{y=1}^N \frac{1}{S(x,y)} \left[ S(x,y) - \sum_{i=1}^n \sum_{j=1}^n a_{ij} X_i(x) Y_j(y) \right] X_k(x) Y_l(y) = 0. \dots (4.7)$$

A comparison of 4.7 with 4.6 shows that the equations for the coupled system yield the same least-squares estimate of  $a_{ij}$  as the equation for the original model if  $w_y = 1$  for all  $y$ . This implies that the fits in the second stage based on 4.2b should be unweighted.

(d) Error Estimate

$$\text{Let } \sum_{x=1}^N \sum_{y=1}^N X_k(x) Y_l(y) = V_{kl} \dots (4.8)$$

$$\sum_{x=1}^N \sum_{y=1}^N \frac{X_i(x) Y_j(y) X_k(x) Y_l(y)}{S(x,y)} = C_{ijkl}$$

$$\text{then from 4.7 } [V_{kl}] = [C_{ijkl}] [a_{ij}]$$

$$\text{therefore } a_{ij} = \sum_{kl} C_{ijkl}^{-1} V_{kl} \dots (4.9)$$

$$\text{and } \sigma_{ij}^2 = \text{var}(a_{ij}) = \frac{\chi^2}{f} C_{ijij}^{-1} \dots (4.10)$$

$$\text{where } f = N^2 - n^2$$

$$\chi^2 = \sum_{x=1}^N \sum_{y=1}^N \left( 1/S(x,y) \right) \left[ S(x,y) - \sum_{i=1}^n \sum_{j=1}^n a_{ij} X_i(x) Y_j(y) \right]^2 .$$

But  $C$  is a 4th order  $n$ -dimensional matrix which can be recast into a  $n^2$ -dimensional matrix so for even a reasonable number of gamma rays the inversion to  $C^{-1}$  is next to impossible. Thus the error in the intensity coefficients cannot be practically determined.

Returning to the coupled equations, in the first stage, if we let

$$v_k = \sum_x X_k(x) \quad \dots(4.11)$$

and 
$$T_{ik} = \sum_{x=1}^N X_i(x) X_k(x) / S(x, y)$$

then from 4.3 
$$a_i(y) = \sum_k T_{ik}^{-1} v_k \quad \dots(4.12)$$

Similarly, in the second stage, let

$$u_{il} = \sum_y Y_l(y) a_i(y) \quad \dots(4.13)$$

and 
$$U_{jl} = \sum_{y=1}^N Y_j(y) Y_l(y)$$

then from 4.4 
$$a_{ij} = \sum_l U_{jl}^{-1} u_{il} \quad \dots(4.14)$$

On substituting into 4.14 from 4.11 to 4.13 we get

$$\begin{aligned} a_{ij} &= \sum_l U_{jl}^{-1} \left[ \sum_y Y_l(y) \left[ \sum_k T_{ik}^{-1} \cdot \sum_x X_k(x) \right] \right] \\ &= \sum_k \sum_l U_{jl}^{-1} \left[ \sum_x \sum_y T_{ik}^{-1} Y_l(y) X_k(x) \right] \quad \dots(4.15) \end{aligned}$$

If  $T_{ik}^{-1}$  is replaced by the average value  $\bar{T}_{ik}^{-1}$  then we can

substitute 4.8 in 4.15 to give

$$a_{ij} \doteq \left[ \sum_k \sum_l U_{jl}^{-1} \bar{T}_{ik}^{-1} \right] v_{kl} \quad \dots(4.16)$$

and 
$$\sigma_{ij}^2 \doteq \frac{\chi^2}{f} U_{jj}^{-1} \bar{T}_{ii}^{-1} \quad \dots(4.17)$$

Since  $T_{ik}$  and  $U_{jl}$  are  $n \times n$  matrices where normally  $n \leq 10$ , the inverses are readily established and an estimate of the error in the intensity coefficients is now possible.

It remains now to determine the relationship between the approximate and the exact variance. This is at present under study.

(e) The Physical Significance of the Variance

The variance of  $a_{ij}$  is  $\sigma_{ij}^2$  where  $\sigma$  is called the standard deviation. The standard deviation represents a measure of the width of the distribution curve for  $a_{ij}$ . If we assume the probability curve is a Gaussian centered with mean value at the origin then  $P(a_{ij}) = P(z)$  is given by

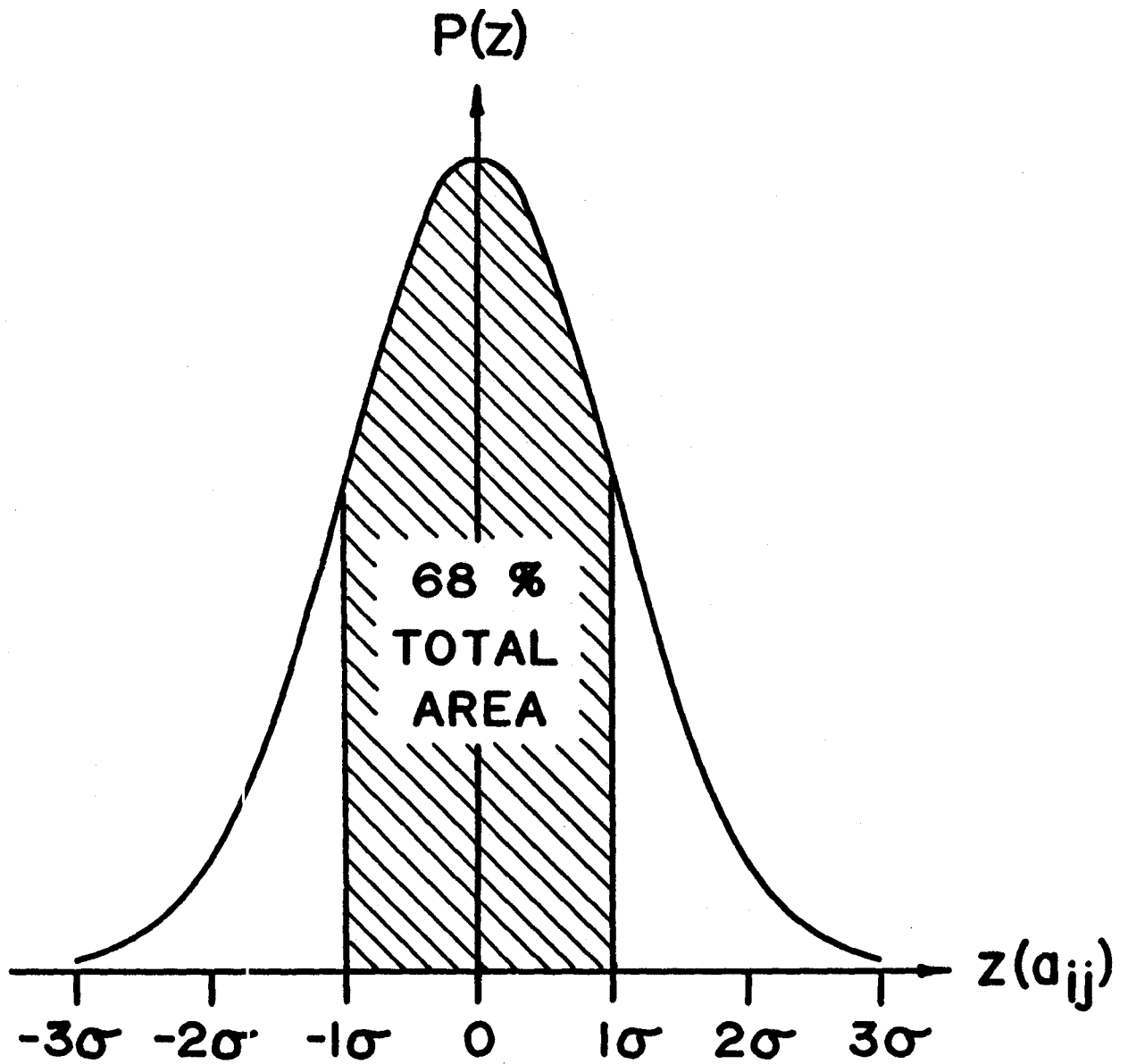
$$P(z) = \frac{e^{-z^2/2\sigma^2}}{\sqrt{2\pi}\sigma} .$$

As Figure 19 illustrates, 68% of a particular  $a_{ij}$  value lies between  $\pm\sigma$ . Hence the smaller the  $\sigma$  or the  $\sigma^2$  (variance) then the more peaked is the probability distribution and the more reliable the value obtained for  $a_{ij}$ .

#### 4.2 Intensities from Intensity Correlation Matrix

Before the single gamma-ray intensities can be determined, the correlation intensities must first be found. To do this the first row and column of the coincidence surface  $S(x,y)$  is replaced with a corresponding single run at the same gain but not necessarily normalized in time. Using a computer, the singles intensity coefficients  $b_i$  and  $c_j$  (the number of times the line shapes  $X_1(x)$  and  $Y_j(y)$  fit into the single spectra  $S(x,1)$  and  $S(1,y)$  respectively) are found. From the rest of the response surface, the intensity correlation coefficients  $a_{ij}$  (the number of times the response surface  $X_1(x)Y_j(y)$  fits into the coincidence surface  $S(x,y)$  for the  $i$ - $j$  coincidence)

FIGURE 19



ERROR CURVE

are obtained.

If we let  $N_s$  and  $N_c$  be the sample source strength for the time run for the singles and coincidences respectively,  $P$  the probability of gamma decay,  $e$  the detector efficiency, and  $k$  the normalization constant for the line shape, then it follows for coincident gamma rays  $\gamma_i$  and  $\gamma_j$

$$\left. \begin{aligned} a_{ij} &= N_c P(\gamma_i \gamma_j) e(\gamma_i) e(\gamma_j) k(\gamma_i) k(\gamma_j) \\ b_i &= N_s P(\gamma_i) e(\gamma_i) k(\gamma_i) \\ \text{and } c_j &= N_s P(\gamma_j) e(\gamma_j) k(\gamma_j) \end{aligned} \right\} \dots (4.18)$$

It is now obvious that the ratio of the product of the singles intensity coefficients to the intensity correlation coefficients will be independent of detector efficiencies and line shape normalization, viz:

$$\frac{b_i c_j}{a_{ij}} = K \frac{P(\gamma_i) P(\gamma_j)}{P(\gamma_i \gamma_j)} \dots (4.19)$$

where  $K$  is a constant.

The computer can be programmed to find the intensity correlation matrix  $b_i c_j / a_{ij}$ . Then by examining the decay scheme of the element under study, the value of the various probabilities  $P$  can be determined from the theoretical intensities of the gamma rays. These theoretical intensities are in terms of several parameters, the number required being one less than the maximum number of gamma rays needed to form a cascade from the highest to the lowest energy level. Hence a theoretical intensity correlation

matrix can be set up. Elements  $a_{ij}$  where  $i-j$  is not a coincident gamma pair will be zero.

Now the theoretical and experimental matrix elements can be equated and from the resulting equations the intensity parameters can be found. Practically, since the theoretical matrix is symmetrical and because several of the elements are identical, then the corresponding computed elements can be averaged, reducing the number of equations required to solve. Once the parameters have been found, the individual gamma-ray intensities can be worked out and also their probable errors.

#### 4.3 Br<sup>82</sup> Gamma-Ray Intensities

##### (a) Data Collection

In the case of Br<sup>82</sup>, let the probabilities of the 554-, 619-, and 698-keV gamma rays decaying be  $x, y$ , and  $z$  respectively. Thus  $x, y$ , and  $z$  are the theoretical intensity parameters mentioned in the previous section. If we assume that the 220- and 1648-keV gamma rays have negligible intensity, then the theoretical intensity correlation matrix will be in terms of  $x, y$ , and  $z$  as indicated in Table III on page 48.

TABLE III

Theoretical Intensity Correlation Matrix  
(Each element shown has been divided by the constant K)

	554	619	698	777	827	1044	1317	1475
554	0	x	x	$\frac{xq^*}{q+x-1}$	0	0	x	x
619	x	0	y	$\frac{yq}{z}$	0	0	0	y
698	x	y	0	q	0	0	0	0
777	$\frac{xq}{q+x-1}$	$\frac{yq}{z}$	q	0	q	q	q	0
827	0	0	0	q	0	1-x	0	0
1044	0	0	0	q	1-x	0	0	0
1317	x	0	0	q	0	0	0	0
1475	x	y	0	0	0	0	0	0

$$* \quad q = 1-y+z$$

The coincidence surface  $S(x,y)$  was a  $32 \times 32$  array with 500- to 1600-keV range along each dimension. The crystals were at  $180^\circ$  and placed about 5 cm. from the source. Coincidence and random adding at this distance was not negligible but these and other spurious events were accounted for in the reduction analysis by including the 1648-keV gamma ray line shape. The sample was counted for an hour. This period of time was short enough to be able to ignore any possible gain shifts in the two

dimensions. The single spectra were run simultaneously for four minutes on the 32x32 array set-up while the analyzer was in a "free" mode. Background spectra were also run for the same time and subtracted to yield  $S(x,1)$  and  $S(1,y)$ .  $S(x,1)$  is plotted in Figure 20.  $S(1,y)$  is almost identical. Also  $\text{Na}^{22}$ ,  $\text{Cs}^{137}$ ,  $\text{Mn}^{54}$ ,  $\text{Zn}^{65}$ , and  $\text{Co}^{60}$  were analyzed separately at the same gain to produce standard lines from which the line shapes for stripping could be interpolated.

(b) Preparation of Line Shapes and Surface Reduction

The energy scale for the  $\text{Br}^{82}$  coincidence data is so condensed that each gamma photopeak has a width of just over three channels. These three peak channels and their number of counts  $N$  for the photopeaks of the 554-, 777-, 1044-, 1317-, and 1475-keV gamma rays were found in the X and Y directions from the coincidence array. The other gamma rays were not resolved.

If we assume that the three peak points lie on a Gaussian, then the highest point on the Gaussian, which will be the true channel location for the gamma-ray energy, is found in the following way, with reference to Figure 21.

The natural logarithm of a Gaussian is a parabola. Let  $z = \ln N$ . Then the function  $z$  is a parabola of the form

$$z = ax^2 + bx - c \quad \dots (4.20)$$

FIGURE 20

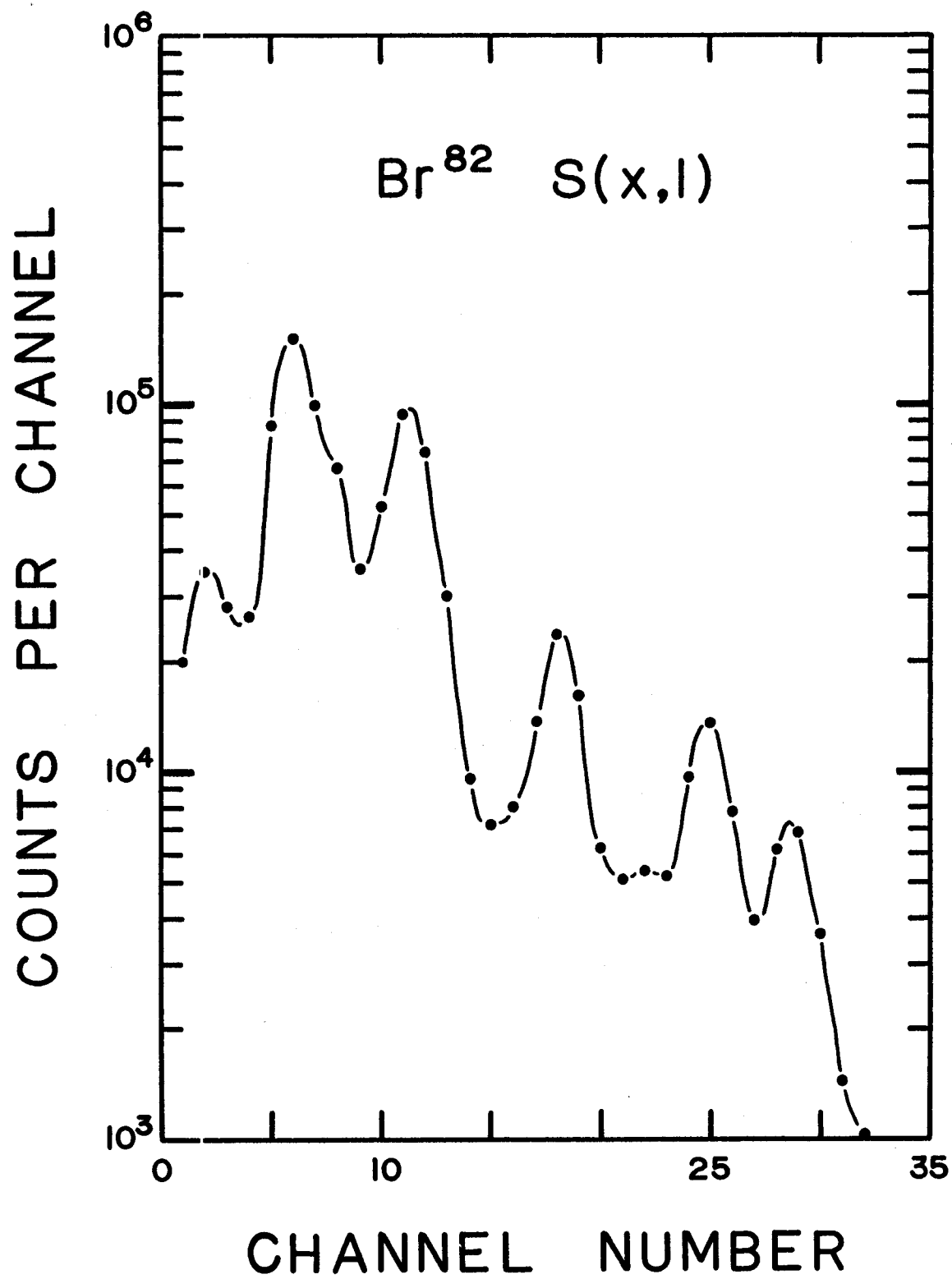
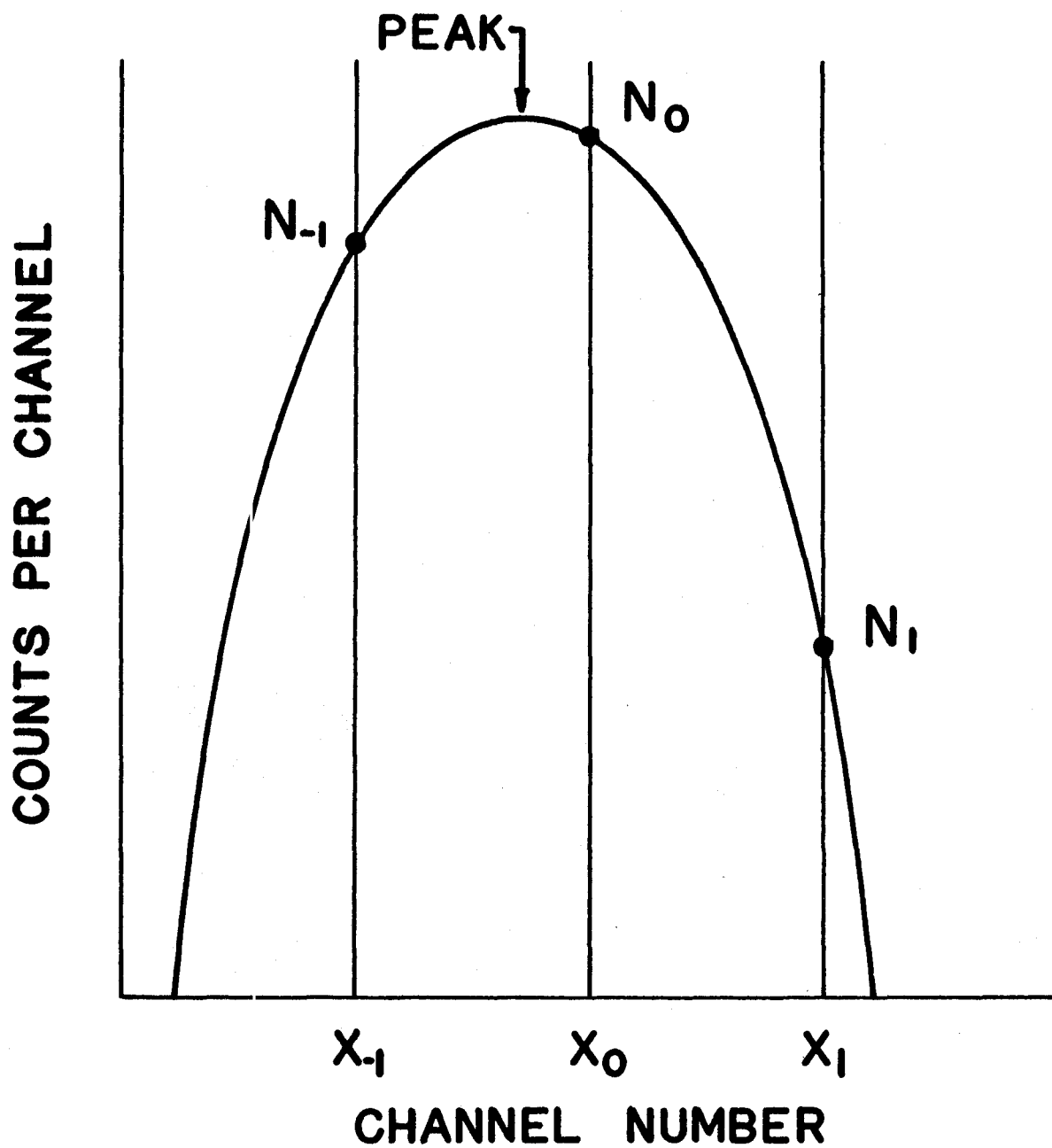


FIGURE 21



GAUSSIAN PEAK LOCATION

Therefore we can say

$$\left. \begin{aligned} z(x=-1) &= z_{-1} = a - b + c \\ z(x=0) &= z_0 = c \\ \text{and } z(x=1) &= z_1 = a + b + c \end{aligned} \right\} \dots (4.21)$$

Solving we find that

$$a = (1/2)(z_{-1} + z_1 - 2z_0) = (1/2) \ln \left( \frac{N_1 N_{-1}}{N_0^2} \right) \dots (4.22)$$

$$\text{and } b = (1/2)(z_1 - z_{-1}) = (1/2) \ln \left( \frac{N_1}{N_{-1}} \right) \dots (4.23)$$

For a maximum,  $\frac{dz}{dx} = 2ax + b = 0$ .

Therefore the peak is at

$$x = -\frac{b}{a} = -1/2 \frac{\ln(N_1/N_{-1})}{\ln(N_1 N_{-1}/N_0^2)} \dots (4.24)$$

Using equations 4.22 to 4.24 the values  $x$ ,  $a$ , and  $b$  were calculated for the resolved gamma rays. After converting the gamma energies to NaI pulse heights using Heath's curve for the non-linearity of NaI (11), a plot of pulse height versus  $x$  and  $1/a$  was constructed for both X and Y dimensions. Using the least squares condition, the equations of the best straight lines through the points were found and interpolations at the pulse heights of the unresolved gamma rays (619, 698, 827, and 1648 keV) were made to find their  $x$  and  $1/a$  values. From this  $b$  was readily calculated. Choosing an arbitrary  $c$  value, from equations 4.21 the  $z$  values were determined. Then using the relation  $N = e^z$ , the three peak counts for the unresolved gamma rays were obtained. Finally, the rest of the line shape for all the gamma rays was interpolated from the standard lines.

The reduction of the coincidence surface was then carried out using the McMaster IBM 7040 Computer. The operation was programmed so that  $a_i(y)$ ,  $a_{ij}$ , with their respective residuals and  $\chi^2$  as well as  $b_i c_i / a_{ij}$  were printed out. By plotting  $a_i(y)$  for all  $y$ , true coincidence spectra for each gamma ray were obtained. Comparisons between the locations of the gamma rays in these spectra to the locations in the line shapes pointed out small errors in positioning of the line shapes in the Y dimension. These were shifted accordingly. By transposing the  $S(x,y)$  data to  $S(y,x)$  and interchanging the X-and Y-line shapes, a rerun of the program produced  $a_j(x)$  and as with the Y-line shapes, the X-line shapes were shifted to more exact positions.

With the corrected line shapes, the program was run again keeping a careful check on the residuals. Small alterations were repeatedly made in the line shapes until the residuals were as small as possible. In the final run the average value of  $\chi^2/f$  for the  $a_i(y)$  was 11.

### (c) Results

Table IV lists the average value for the different matrix elements. The error quoted is the probable error in the mean.

TABLE IV  
Matrix Element Values

Parameter	No. Times in $a_{ij}$	Average Value	Error
Kx	8	3.07	$\pm 10 \%$
$K(1-x)$	2	1.15	$\pm 1 \%$
Ky	4	1.53	$\pm 16 \%$
Kq	8	3.16	$\pm 13 \%$
$K\left(\frac{xq}{q+x-1}\right)$	2	6.33	$\pm 2 \%$
$K\left(\frac{yq}{z}\right)$	2	8.20	$\pm 22 \%$

Solving for x, y, and z yields:

$$x = 0.73 \pm 13 \%$$

$$y = 0.43 \pm 12 \%$$

$$z = 0.14 \pm 31 \%$$

The resulting gamma-ray intensities are as follows in Table V.

TABLE V  
Br<sup>82</sup> Intensities from Regression Analysis

Gamma Energy keV	Theoretical Intensity	Calculated Intensity	Intensity Based On 777 = 100	Intensity from Data Cards (1)
554	x	0.73 <sup>+13%</sup>	103 <sup>+14</sup>	78-105
619	y	0.43 <sup>+12%</sup>	61 <sup>+8</sup>	50
698	z	0.14 <sup>+31%</sup>	20 <sup>+6</sup>	33-37
777	1-y+z	0.71 <sup>+16%</sup>	100 <sup>+16</sup>	100
827	1-x	0.27 <sup>+38%</sup>	38 <sup>+15</sup>	28-30
1044	1-x	0.27 <sup>+38%</sup>	38 <sup>+15</sup>	28-36
1317	x-y	0.30 <sup>+37%</sup>	42 <sup>+16</sup>	24-36
1475	y-z	0.29 <sup>+24%</sup>	41 <sup>+10</sup>	11-21

#### 4.4 Conclusions

A comparison of the Nuclear Data Card (1) intensity values and the intensity values found earlier in this report by other methods (see Table II) with those determined from the surface stripping reveals that the majority of the values agree to within the probable error. If the intensity value of z could be increased, then this would tend to increase the intensity of the 698- and 777-keV lines and decrease the intensity of the 1475-keV line. This is exactly what is required to bring these new results closer to the Data Card values. An inspection of the Br<sup>82</sup> single spectrum S(x,1), Figure 20, shows that the 698-keV line is not resolved so that the stripping of the single

and coincidence spectra will definitely tend to be unreliable at best for this gamma ray. This holds true for the 619-keV gamma ray as well. The intensity of the 1475-keV line depends, in the regression analysis method, on the intensities of the 619- and 698-keV lines, y and z respectively. Since these three gamma rays have the largest discrepancy in intensity values, it is apparent that this method for the extraction of intensities works best when the gamma rays are resolved.

However, considering the large number of gamma rays analyzed and the large energy range covered by the 32 channels, the success of the regression analysis for  $\text{Br}^{82}$  testifies to the usefulness of this straightforward method of obtaining reliable intensity values. If a similar analysis were to be made using, say, a 100x100 coincidence array where all intense photopeaks were resolved, intensity values to within a few per cent could be obtained readily.

## REFERENCES

1. Nuclear Data Sheets, compiled by K. Way et al.  
(National Academy of Sciences - National  
Research Council, Washington 25, D. C.)
2. T. J. Kennett, W. V. Prestwich and G. L. Keech,  
submitted to Nucl. Instr. and Methods (1964)
3. H. I. West, Jr., Phys. Rev. 101, 915 (1956)
4. R. D. Evans, The Atomic Nucleus, McGraw-Hill  
(1955) p. 706
5. R. D. Evans and R. O. Evans, Rev. Mod. Phys. 20,  
305 (1948)
6. J. W. Dewdney, Nucl. Phys. 43, 303 (1963)
7. Fay Ajzenberg-Selove, Nuclear Spectroscopy - Part B,  
Academic Press (1960) p. 1013
8. C. S. Han and N. B. Gove, Nuclear Data Sheets,  
Nov. 1963
9. R. D. Evans, The Atomic Nucleus, McGraw-Hill  
(1955) p. 560
10. N. Benczer-Koller, Bull. Am. Phys. Soc. 1,  
41 (1956)
11. R. L. Heath, Data Analysis Techniques for Gamma-  
Ray Scintillation Spectroscopy  
AEC Report IDO - 16784 (1962)